LA-ICP-MS U-Pb carbonate geochronology: strategies, progress and limitations

Nick M W Roberts[1], Kerstin Drost[2], Matthew S A Horstwood[1], Daniel J Condon[1], David Chew[2], Henrik Drake[3], Antoni E Milodowski[4], Noah M McLean[5], Andrew J Smye[6], Richard J Walker[7], Richard Haslam[4], Keith Hodson[8], Jonathan Imber[9], Nicolas Beaudoin[10], Jack K Lee[9]

[1]Geochronology and Tracers Facility, British Geological Survey, Environmental Science Centre, Nottingham, NG12 5GG, UK
[2]Department of Geology, Trinity College Dublin, Dublin 2, Ireland
[3]Department of Biology and Environmental Science, Linnaeus University, 39231 Kalmar, Sweden
[4]British Geological Survey, Environmental Science Centre, Nottingham, NG12 5GG, UK
[5]Department of Geology, University of Kansas, Lawrence, KS 66045, USA
[6]Department of Geosciences, Pennsylvania State University, University Park, PA 16802, USA
[7]School of Geography, Geology, and the Environment, University of Leicester, Leicester, LE1 7RH, UK
[8]Department of Earth and Space Sciences, University of Washington, Seattle, WA 98195, USA
[9]Department of Earth Sciences, Durham University, Science Labs, Durham, DH1 3LE, UK
[10]Laboratoire des Fluides Complexes et leurs Réservoirs-IPRA, E2SUPPA, Total, CNRS, Université de Pau et des Pays de l'Adour, UMR5150, Pau, France

Words: ca. 13500
Figures: 15
Tables: 0
References: 135
Supplementary files: 2

Abstract

Laser Ablation Inductively Coupled Plasma Mass Spectrometry (LA-ICP-MS) U-Pb geochronology of carbonate minerals, calcite in particular, is rapidly gaining popularity as an absolute dating method. The high spatial resolution of LA-ICP-MS U-Pb carbonate geochronology has benefits over traditional Isotope Dilution methods, particularly for diagenetic and hydrothermal calcite, because uranium and lead are heterogeneously distributed on the sub-mm scale. At the same time, this can provide limitations to the method, as locating zones of radiogenic lead can be time-consuming and 'hit or miss'. Here, we present strategies for dating carbonates with in situ techniques, through imaging and petrographic techniques to data interpretation; our examples are drawn from dating of fracture-filling calcite, but our discussion is relevant to all carbonate applications. We review several limitations to the method, including open system behaviour, variable initial lead compositions, and U-daughter disequilibrium. We also discuss two approaches to data collection: traditional spot analyses guided by petrographic and elemental imaging, and image-based dating that utilises LA-ICP-MS elemental and isotopic map data.

1. Introduction

Calcite ($CaCO_3$), along with other carbonate minerals (e.g. aragonite, dolomite, magnesite), forms in a wide variety of geological environments as both a primary and secondary mineral phase, including diagenetic, biogenic, igneous, metamorphic and hydrothermal environments. Calcite can incorporate uranium upon its formation, making it a potentially suitable chronometer for U-Pb and U-Th geochronology. Calcite geochronology therefore has the potential to provide direct timing constraints to a broad suite of geoscience applications. Calcite has been dated in the past by chemical dissolution and isotope dilution (ID) with measurement by either Thermal Ionisation Mass Spectrometry (TIMS) or Inductively Coupled Plasma Mass Spectrometry (ICP-MS) (e.g. Smith and Farquhar, 1989; DeWolf and Halliday, 1991; Brannon et al., 1996; Rasbury et al., 1997; Richards et al., 1998; Woodhead et al., 2006; Pickering et al., 2010), collectively referred to here simply as Isotope Dilution (ID). More recently, there has been a proliferation in the use of laser ablation (LA-) ICP-MS applied to calcite geochronology (Li et al., 2014; Coogan et al., 2016; Roberts & Walker, 2016, Ring & Gerdes, 2016; Methner et al., 2016; Goodfellow et al., 2017; Burisch et al., 2017, 2018; Drake et al., 2017, 2019, 2020; Hansman et al., 2017;

Hellwig et al., 2018; Godeau et al., 2017; Beaudoin et al., 2018; Drost et al., 2018; Mangenot et al., 2018; Nicholson et al., 2020; Nuriel et al., 2017, 2019; Parrish et al., 2018; Walter et al., 2018; Yokoyama et al., 2018; Smeraglia et al., 2019; Holdsworth et al., 2019; MacDonald et al., 2019; Scardia et al., 2019). Presently, we are not aware of successful secondary ion mass spectrometry (SIMS) U-Pb dating of carbonate mineralisation, but this presents an alternative microbeam method to LA-ICP-MS.

The first review of the possibilities for carbonate geochronology was published by Jahn & Cuvellier (1984), and this was substantially updated by Rasbury & Cole (2009). The latter provided up-to-date discussion on U-Pb isotope systematics in carbonates, particularly regarding Pb-Pb and U-Pb isochron methods, as well as a review of the applications to date. At that time, both marine- (e.g. limestone, dolomite) and meteoric-water sourced carbonates (e.g. speleothems and tufas) had received the most attention, due to their often-favourable uranium contents, and studies of hydrothermal carbonate were scarce (e.g. Brannon et al., 1996; Grandia et al., 2000). U-Pb dating of speleothems has been further reviewed by Woodhead et al. (2006 and 2012), focussing on data generated by ID, and more recently Woodhead and Petrus (2020) discuss the use of LA-ICP-MS for speleothem dating.

Now that microbeam (i.e. LA-ICP-MS and SIMS) U-Pb geochronology is proving to be a useful method for a range of geoscience applications, it is pertinent to address what can be achieved with the method, what the current limitations are, and where improvements can be made in the future. We refer to LA-ICP-MS through the rest of this paper, but acknowledge that nearly all of the points we cover are equally relevant to SIMS methods. The key benefit to LA-ICP-MS dating is that its high spatial resolution can be used to relate U-Pb and other geochemical analyses to imaged textures. This is critical for providing context to the obtained dates. Carbonate materials are heterogeneous in composition elementally, isotopically, and texturally. These factors can all lead to scatter in U-Pb data, and will often hinder the ability to generate high precision (i.e. <1% 2σ) U-Pb dates. In fact, after propagation of all relevant uncertainties, final LA-ICP-MS U-Pb dates typically exceed 3% precision (2σ). For this reason, LA-ICP-MS carbonate U-Pb geochronology is particularly suited for applications in tectonics and crustal fluid-flow, but commonly less suited for applications in stratigraphy and palaeoclimate.

Here we present a review of LA-ICP-MS U-Pb carbonate geochronology, focusing on its benefits, application and limitations. We pay particular attention to hydrothermal and diagenetic carbonates; these can constrain the ages of mineral systems, crustal deformation and fluid-flow, and represent a significant growth area for this method. Using several case studies, we highlight the utility of image-guided analysis, where various imaging techniques provide critical context for interpreting U-Pb data. We also provide case studies for an age-mapping technique that is an alternative to traditional static spot ablation, and can be used in combination with sample imagery to generate U-Pb age data. Finally, we highlight issues surrounding initial lead compositions, initial disequilibrium in the U-Pb system and open-system behaviour.

2. LA vs ID strategies

Geochronology by ID provides the most accurate assessment of the U-Pb age of a sample, through use of calibrated isotopic tracer solutions, but it is time-consuming and requires a clean laboratory facility for sample dissolution and column chemistry. The spatial resolution of ID is typically much lower than that offered by microbeam techniques, although resolution can be increased by using a high precision micro-drill for direct sampling. A major limiting factor is that carbonate materials typically have very low U concentrations (ca. 10 ppb to 10 ppm U) compared with traditional U-bearing accessory minerals (e.g., often >100 ppm U in zircon). This means that samples with low Pb concentrations yield higher blank/sample ratios, hindering the accuracy and precision of the resulting data, and secondly that the comparatively large volumes of material needed for ID analyses result in an ‘averaging’ effect and reduction of spread in U/Pb space.

LA-ICP-MS is a much quicker technique than ID, and therefore less expensive per analysis. Several samples can be run in a single day, meaning the technique is ideal for screening of large sample sets to find the most suitable material. The effect of blanks sourced from dissolution and chemical purification is negated, and very low (<100 ppb) Pb contents can be analysed. However, LA-ICPMS is generally less precise analytically compared to ID approaches. Another major limitation is the need to normalise to a matrix-matched reference material. This means that the uncertainty of the reference material becomes a limiting uncertainty, and matrix effects between materials of different composition will generate scatter and/or bias in the U-Pb dates that are difficult to correct for.

The biggest benefit of LA-ICP-MS comes from the spatial resolution (less than ca. 100 μm) at which data can be obtained, particularly given the length scales of uranium concentration heterogeneity in carbonate. We find that for hydrothermal and diagenetic calcite in particular, uranium is heterogeneously distributed across veins and vein phases, and within individual crystals (see Figure 1). Uranium concentration heterogeneity typically spans 1 to 3 orders of magnitude, with the length-scale of this variation being commonly much less than 1 mm. Targeting of high U domains is therefore difficult without a high spatial-resolution sampling method. Intracrystalline uranium distributions within calcite define several patterns (see Figure 1): concentrated along cleavage planes (a), growth-zone controlled (c, d and f), concentrated towards grain rims (areas of b and e), and with apparent disorder (areas of b and e). Laser ablation has the spatial resolution capable of targeting such elemental (and isotopic) zonation, making it easier to avoid distinguishable alteration zones and inclusions at the 10-100 μm scale.

Figure 1 here.

For common-lead bearing minerals such as calcite, the extreme range in parent/daughter ratios encountered (quoted here as ^{238}U divided by initial lead as ^{204}Pb; a ratio known as μ), means that ID does not always lead to an improvement in precision on the regressed age. This is demonstrated by the schematic model in Figure 2. Sampling for ID provides an average of elemental and isotopic zonation within the analytical volume, perhaps >1 mm^3, depending on the concentration of U and Pb within the crystal(s). The resulting data should be precise (depending on the sample/blank ratios), but may potentially have a small spread in parent/daughter ratios (i.e. $^{238}U/^{206}Pb$) due to the averaging effect during sampling. In contrast, LA sampling has the potential to target and utilise such zonation, better resolving end-member μ compositions, and resulting in analyses with a greater spread in $^{238}U/^{206}Pb$ ratios. This potentially improves the resolving power of a regression of the measured isotopic ratios allowing definition of, ideally, the high-μ (radiogenic lead) and low-μ (initial lead) end-member compositions of the data array (see Figure 2). Along with the generally high-*n* datasets generated by the LA-ICP-MS approach, these well-constrained regressions can result in similar precision for $^{206}Pb/^{238}U$ ages than those using ID data alone.

Insert Figure 2 here:

When calculating an age and uncertainty from a regression/isochron, it is assumed that: 1) the dataset describes a single age population whose variability or scatter is derived solely from the analytical process 2) each analysis represents a closed system, and 3) all analyses share the same initial Pb isotope composition. When these assumptions are satisfied, the MSWD should be about 1 (Mean Squared Weighted Deviation; Wendt and Carl, 1991). LA-ICP-MS data-points generally have a lower precision than those derived by ID. These lower precision data-points can mask scatter that exists within the level of the data-point uncertainties. This caveat must be considered when interpreting regressed data (or weighted means). In other words, age interpretations rely on isochron assumptions that can only be resolved at the level of the data-point uncertainties. More precise ID data, therefore, have better resolution of scatter and better constrain the likelihood that a sample does not comprise a single population. However, sampling for ID can also contribute to this scatter by analysing larger amounts of material, with a greater chance of including altered zones or zones from different generations. For applications where the best possible precision is needed (e.g. for stratigraphic constraints or characterisation of potential U-Pb carbonate reference materials), a workflow involving both LA-ICP-MS dating followed by ID on the most favourable material is likely to be the most effective. For applications where the required precision is on the order of several percent, image-guided LA-ICP-MS without ID is suitable.

3. Identifying suitable carbonate material for dating

3.1. μ ($^{238}U/^{204}Pb$) in carbonate

An 'ideal' U-Pb chronometer requires incorporation of U (the parent isotopes ^{238}U and ^{235}U which decay to ^{206}Pb and ^{207}Pb respectively), and zero or low concentrations of initial (or 'common') Pb during its formation; this is typically expressed as the ratio of parent uranium to initial Pb - $^{238}U/^{204}Pb$, or μ. In addition, both the parent and daughter isotopes ideally remain a closed system from formation until present-day. Many chronometers lack these ideal criteria but still provide successful materials for dating: the subset of 'common-lead bearing chronometers' comprise small to large initial lead concentrations that are of uniform composition (e.g. titanite, apatite). The ideal criteria are generally rare in carbonates, but

many carbonate materials from a range of different geological environments are successful common-lead bearing chronometers. Rasbury and Cole (2009) showed that carbonates of meteoric origin have the highest μ values, and hydrothermal varieties the lowest, with marine varieties in the middle (see Supplementary Figure S1). However, the recent literature on calcite dating demonstrates that with careful characterisation and sampling, high μ domains can be found in a range of hydrothermal and diagenetic calcite.

The amount of U needed to generate an age is dependent on two factors: (1) the age of the material and (2) the initial μ ratio of the material. The younger a sample is, the less time there is for the growth of radiogenic daughter Pb from parent U. With a higher μ, the ratio of measured radiogenic Pb to common (initial) Pb will be higher, giving greater confidence and (in general) precision and accuracy to the resulting age determination. The effect of these factors is shown in Figure 3. Two Tera-Wasserburg plots are shown, with isochrons for samples of different ages (100 to 10 Ma on the left, 1000 to 100 Ma on the right). The most accurate and precise age determinations, i.e. those that can be interpreted with most confidence, are generated when the sample comprises abundant radiogenic lead, i.e. gets close to the lower part of the concordia curve where the regression intercepts. Each plot shows regressions for individual samples between a common-lead composition (~0.8) and a radiogenic end-member (with the age labelled). The colour-coded points along each regression reflect the amount of radiogenic lead that will be created by decay of ^{238}U, based upon the given μ value. For example, utilising the left plot, a sample of 15 Ma, with a μ of 10,000, will have a measured $^{207}Pb/^{206}Pb$ of ~0.4, equalling about a 50:50 ratio between radiogenic and initial lead. To get a near concordant measurement of this sample would require a μ value of over 200,000. These plots demonstrate that when simply regarding the abundance of radiogenic lead, older samples are more amenable to dating than those young in age. The preservation of a closed isotopic system over long time periods is what makes dating old samples (i.e. Precambrian materials) potentially difficult.

Insert Figure 3 here:

When absent of concordant analyses, both high μ and a significant spread in initial μ values are required to generate the most robust ages, as these will pin the isochron at the radiogenic end-member with greater confidence. Some calcite exhibits sufficiently high μ to generate concordant data (e.g. Richards et al., 1998; Roberts & Walker, 2016; Nuriel et al.,

2017); these ages do not heavily rely on the composition of the common lead end-member, but such ages are rare with a material that so commonly exhibits high initial lead abundances. Ages can be derived from isochrons with low amounts of radiogenic lead, i.e. those with low μ. Such isochrons can be regressed to provide lower intercept ages, but the confidence in these ages is subject to having well-behaved data conforming to a single population, requiring precise data-point uncertainties (e.g. Figure 4g). Such low μ isochrons can potentially give imprecise and even inaccurate lower intercept ages, and thus confirmation through multiple samples and/or alternative age constraints are favoured.

In Figure 4, we present a selection of 'real-world' data to highlight the potential complexity of carbonate U-Pb data. These data from natural samples broadly range from undesirable to most desirable from a to i, with the following notable characteristics:

(a) Dominated by common lead with large data-point uncertainties (due to low count-rates) that hamper the distinction between open-system behaviour and radiogenic ingrowth of lead.

(b) All analyses are ca. 100% common lead, with high count-rates providing a precise measurement of the composition of this common lead.

(c) Mixed and scattered data that do not fall on a single linear isochron. This is likely caused by open system behaviour, potentially involving both addition and subtraction of parent ^{238}U.

(d) Majority of data define a linear array with a large spread in U/Pb ratios. Some other analyses fall on a horizontal array, suggesting they experienced open-system behaviour (e.g., local ^{238}U mobility).

(e) Data form an apparent single linear array, but large uncertainties (due to low count-rates) may obscure mixed ages or minor open-system behaviour.

(f) Dominated by relatively radiogenic isotopic compositions, but with large data point uncertainties due to low count-rates. The narrow range in μ leads to a large age uncertainty from extrapolating to the lower concordia intercept. The age uncertainty would be improved with a common lead composition estimated from contemporaneous low-μ samples of the same suite.

(g) A short isochron, termed a 'small scale isochron' by Ring & Gerdes (2016). There are no radiogenic isotopic compositions to anchor the extrapolation to a lower intercept concordia date, but a tight data array yields a realistic intercept age.

(h) Dominated by radiogenic isotopic compositions, and the spread in the array provides a precise lower intercept date; small data-point uncertainties improve ability to identify potential outliers.

(i) A precise regression due to well-behaved closed system behaviour, high count rates giving small uncertainties, and a large spread in U/Pb ratios providing a precise estimate of both the age and the common lead isotopic composition.

Insert Figure 4 here:

3.2. U and Pb contents in carbonate

At present, there is a lack of predictive criteria that can be used in the field or in the laboratory to screen samples prior to analysis for high μ domains. Radionuclide incorporation in calcite is not well understood despite several decades of interest, primarily driven by the field of nuclear waste storage and characterisation (e.g. Langmuir, 1978; Milton & Brown, 1987; Sturchio et al., 1998; Reeder et al., 2000, 2001; Kelly et al., 2003; Weremeichik et al., 2017; Drake et al., 2018). This is because trace element incorporation in calcite does not rely on thermodynamically determined partition coefficients, but by a large number of phenomenological variables, including: trace element availability, calcite growth rate, temperature, pH, Eh, pCO_2 and the Ca^{2+}:CO_3^{2-} ratio in solution, ionic size, and U complexation. Furthermore, different trace elements can be preferentially incorporated into structurally different growth steps and faces of growing calcite crystals (Paquette and Reeder, 1995; Reeder, 1996).

Rasbury and Cole (2009) provided a geochronology-focused review of U and Pb in calcite, and we note the following salient features: 1) Pb is both particle reactive and relatively insoluble; 2) Pb is found at very low levels in most fluids (ppt-ppb), providing high Ca/Pb ratios; 3) Pb can substitute for Ca in the crystal lattice, although the Pb cation is larger – ionic radii of Ca^{2+} and Pb^{2+} in six-fold coordination are 114 and 133 pm, respectively; 4) U exists in multiple oxidation states, and its solubility is strongly affected by Eh and pH; and 5) both U(VI) and U(IV) states have been found in calcite, but not with both states together in the same sample.

Points 4 and 5 above are important for understanding why and when uranium is incorporated into calcite, and whether remobilisation is likely. Sturchio et al. (1998), using a combination of X-ray absorption spectroscopy and X-ray microprobe fluorescence, demonstrated that the uranium in a sample of spar calcite was in the form of U(IV), and that U(VI) was less likely based on size and ionic structure (ionic radii of U(IV) and U(VI) in six-fold coordination are 103 and 93 pm, respectively). Given that U(IV) is less mobile than U(VI), this study provided important support for U-daughter geochronology. Kelly et al. (2003) however, found that U(VI) as uranyl (UO_2^{2+}) was the dominant species in a natural sample of vein calcite, which they considered to be more representative of typical low-U material than the Sturchio sample. Drake et al. (2018) found much higher concentrations of uranium in calcite precipitated from deep anoxic groundwater than experimental determinations that were performed in oxic conditions, and interpreted this high uranium uptake as due to incorporation of U(IV) and thus that the partition coefficient for U(IV) in these environmental conditions is orders of magnitude larger than for U(VI). It is evident that more data from natural carbonates in different settings are needed to more fully understand the controls on U and Pb incorporation.

We have compiled uranium and lead concentration data from carbonates analysed in the BGS laboratory over several years (Figure 5). From our data, we see that median U and Pb_{total} concentrations are 1.9 and 0.003 ppm, respectively. Diagenetic carbonate has the second highest median uranium content (0.4 ppm), but also has high Pb content (0.35 ppm). Veins in both terrestrial and Mid-Ocean Ridge settings have low U and Pb contents, with median values well below 100 ppb for both. Biogenic samples, although a smaller dataset, have low contents of U and Pb, generally lower than diagenetic material. Note that this compilation presents total Pb contents, and includes radiogenic Pb as well as initial Pb. The samples in Figure 5 are mostly younger than 200 Ma, or < 4 Ma for the speleothems. The concentration data and U/Pb ratios demonstrate that speleothems in general are much more amenable to U-Pb geochronology, which is why they have been the main focus for this method until the last few years. Dating diagenetic and vein-fill calcite, with more variable and lower contents of U, and higher contents of Pb, have a lower chance of success than speleothems (although it should be noted that the speleothems in general have already been visually pre-screened during sampling).

Insert Figure 5 here:

Ideally, a predictive framework could be constructed to aid field sampling and laboratory-based sub-sampling of carbonate material for geochronological analyses. However, given the large number of variables controlling U and Pb in carbonate, it is unlikely that such a tool can be developed without measuring a large number of parameters in the mineralising/diagenetic system. Relevant information might include the redox history of the system. For example, oxidising fluids may mobilise U as U(VI), which is soluble in hydrous fluids, leading to U loss during fluid-mineral interaction. Conversely, U may undergo much higher precipitation into the mineral phase at redox fronts representing reducing conditions, since reduced U(IV) has lower solubility. Other pertinent information for predicting success includes the nature of the host rock and the source of the fluids. For example, if the mineralising fluids transmit through Pb-rich units, then an undesirable enrichment in the fluid Pb/Ca may potentially take place, leading to lower initial $^{238}U/^{204}Pb$.

The complex nature of trace element uptake, including Pb and U, in carbonate mineralisation is exemplified by recent studies in hydrothermal settings. Fracture mineralisation in the crystalline basement of southern Sweden has been investigated extensively to evaluate potential geological nuclear waste repository facilities. Several studies have shown that most trace element concentrations vary over an order of magnitude within calcite samples (at the thin section scale), and up to several orders of magnitude across individual fractures (Drake et al., 2012, 2014; Maskenskaya et al., 2014; Milodowski et al., 2018). These authors suggest that: 1) trace element chemistry does not trace the source rock of the metals; 2) the co-variation of most trace elements implies changing metal/Ca ratios in the fracture waters; and 3) in-situ factors affect trace element incorporation, such as microbial activity, metal speciation, crystal habit, water type and co-precipitation of other phases such as barite and pyrite. Our own experience of vein-filling fractures matches these previous studies, as shown for example by the basalt-hosted calcite in the Faroe Islands (see Figure 7).

4. Sample screening, imaging and petrography

As discussed above, it is difficult to predict which carbonate samples are most suitable for U-Pb geochronology. We therefore utilise several methods to screen material, with the aim of limiting the time wasted on unsuitable samples, improving the quality of data that is collected, and enhancing the overall efficacy of LA-ICP-MS U-Pb carbonate geochronology. The purpose of sample imaging is two-fold: it provides important spatial characterisation of U and Pb within the sample and also provides the petrographic and compositional context to assess mineral growth mechanisms and alteration textures that are critical for linking dates to processes.

4.1. Non-destructive techniques

A range of non-destructive imaging techniques are available for sample imaging (see Figure 6), including optical microscopy, cathodoluminescence (CL), back-scattered electron imaging (BSE), charge-contrast imaging (CCI), and etch-track or digital autoradiography techniques. Both reflected light and transmitted light are excellent tools for characterising carbonate minerals; the latter being the mainstay of all petrographic analysis. Features which are usefully distinguished in transmitted light include twinning planes, fluid inclusions and grain boundaries (see Figure 6e). Reflected light is a particularly useful technique for characterising carbonates in polished blocks, when thin sections are not available, and also highlights crystal boundaries, and contrasts between different mineral faces (see Figure 6a and 6b).

In carbonate minerals, CL intensity is related to trace element contents but not specifically U concentration. CL brightness is generally ascribed to a number of emitters, with Mn^{2+} being the most dominant luminescence activator and Fe^{2+} being the dominant luminescence quencher in calcite and dolomite (e.g. Machel, 1985, 2000; Savard et al., 1995), although rare earth elements (REE) such as Eu^{2+}, Eu^{3+}, Dy^{3+}, Sm^{3+} and Tb^{3+} along with Pb^{2+} may also activate luminescence in some cases (Richter et al., 2003). Despite not being directly related to U, the very high spatial resolution of CL is useful for identifying µm-scale calcite crystal growth zonation and alteration (Figure 7a and 7b), and for characterising different mineral generations formed from different fluids (e.g. Barnaby & Rimstidt, 1989; Tullborg et al., 2008; Milodowski et al., 2018).

BSE imaging (see Figure 6c and 6d) also does not correlate directly to trace concentrations of uranium, but to the mean atomic number of the mineral. It is useful as an imaging tool for characterising zonation, alteration and growth patterns, although we note that the contrast in zonation largely reflects variations in major element composition, and as such it is typically less sensitive than CL. Ukar & Laubach (2016) provide a recent review of high-spatial resolution SEM-based imaging of vein-filling calcite mineralisation.

CCI under the SEM directly images differences in dielectric properties, which produce charge or conductivity contrasts in the near-surface of the sample that are detected by the secondary electron emission, and may reflect compositional variations or strain induced by deformation (Watt et al., 2000; Robertson et al., 2005).Although the exact origin of charge-contrast is poorly understood, it can provide useful information on crystal growth, compositional zoning and microstructural features (see Figure 6a). It is an underutilised method for geological materials, and has been previously applied to garnet (Cuthbert & Buckman, 2005), feldspar (Flude et al., 2012), limestone (Buckman et al., 2016) and biogenic calcite (Lee et al., 2008). The technique requires very clean and carefully-prepared and polished sample surfaces because it is sensitive to surface contamination and mechanical defects, and imaging needs to be undertaken on uncoated samples under low-vacuum conditions.

In addition to the microscopy-based methods listed above, a lower resolution but potentially useful technique is provided by storage-phosphor imaging-plate (IP) autoradiography using a plastic support film coated with a photostimulated phosphor ($BaFBr:Eu^{2+}$) (Hareyama et al., 2000). This technique records an image of the spatial distribution and intensity of total radioactivity (from alpha, beta and gamma emitters) from a flat sample surface. In natural geological materials, IP radiography records radioactivity from U, Th (and their radioactive daughters), ^{87}Rb, and ^{40}K (Hareyama et al., 2000; Cole et al., 2003). Although U is not specifically discriminated, it has been shown to be a useful screening tool for finding U-bearing domains in carbonate materials (Cole et al., 2005; see Figure 6f). The method has been particularly applied to speleothem studies where its large sample-size capabilities (up to at least 40 cm) are beneficial. Spatial resolution is a few tens of micrometres, depending on the pixel size of the laser scanner. However, the detection limit depends on the exposure time of the IP in direct contact with the sample surface: routinely this is around 14-28 days giving a detection limit of a few ppm U, which is typically higher than many

carbonate samples. Whilst this may be suitable for speleothems, which typically have higher uranium concentrations, we do not regularly adopt the method for very low U contents in vein-filling or diagenetic carbonates.

Fluorescence imaging has long been used in defining and characterising growth fabrics in speleothems, although it does not specifically identify U-rich regions. This usually involves irradiating a sliced sample with UV-light and observing the excited fluorescence emission at a longer (visible light) wavelength, using either a standard UV microscope or digital scanning with a UV laser system (e.g. Shopov et al., 1994; Baker et al., 1995; 2008; Perrette et al., 2005). Fine growth detail with spatial resolutions of between 50 to 100 µm are achievable. Speleothem fluorescence under UV at excitation wavelengths of 300-420 nm is dominated by the intrinsic fluorescence of natural high molecular weight and aromatic organic ("humic" and "fulvic") compounds, with emission between 400-480 nm (Baker et al., 2008). However, we have also successfully imaged speleothems (see Figure 6f) and other geological materials (Field et al., 2019) by direct laser-stimulated scanning fluorescence imaging (LSSFI) using 635 nm (red) and 450 nm (blue) wavelength excitation with 650 nm and 520 nm low-pass wavelength filters, respectively. Although, such equipment is principally applied to imaging of biological materials labelled with organic fluorescent dyes (fluorochromes) (e.g. fluorescein), it is able to image variations in fluorescence originating from organic laminae and subtle differences between carbonate minerals (calcite, aragonite), revealing microtextural details with a resolution of about 100 µm.

Insert Figure 6 here:

4.2. Destructive techniques

Several approaches for destructive sample screening using LA-ICP-MS are available. These can include either systematic or non-systematic (random) spot traverses across carbonate samples, and can include full analyses (i.e. a 30 second ablation following a pre-ablation) or a much shorter analysis time (with or without pre-ablation). We commonly adopt systematic traverses across samples utilising shorter ablation times but including a pre-ablation, so as to avoid common Pb from the surface. This is a quick way to determine with reasonable precision and accuracy whether a sample is a single age population that represents a closed isotopic system with a suitable range in µ. For some samples, this

provides potentially useable age information that does not require any further refinement (e.g. Figure 4h-4i). Conversely, this may provide a population of data that exhibits no potential, i.e. dominated by common-lead (e.g. Figure 5a-5b), open-system behaviour (e.g. Figure 4d), or mixed analyses (e.g. Figure 4c). Screening in this way allows us to analyse several samples or sample-aliquots in a single LA-ICP-MS session, and thus identify the material most likely to provide an accurate and precise age.

Either as an alternative to spot traverses, or subsequent to spot traverses, we use LA-ICP-MS mapping to determine both the location and nature of U and Pb zonation in the carbonate material. Whereas spot traverses provide rapid screening of multiple samples/aliquots, mapping provides fairly rapid (5 x 5 mm in < 2 hours) screening across complexly zoned samples. Different approaches can be adopted, a suite of major and trace elements can be analysed alone, a suite of elements for age determination (i.e. Pb to U ± Hg) can be measured, or, depending on ICP-MS instrumentation, these can be combined, i.e. using a quadrupole ICP-MS (Drost et al., 2018) or a split-stream set-up utilising two ICP-MS instruments (e.g. Kylander-Clark et al., 2013). As will be shown by the examples in the subsequent sections, trace element maps are useful for directly comparing U and Pb zonation with other trace and major elements. We have found that in primary vein-filling calcite, U typically correlates with other trace elements, this varies between samples, but can include V, Mn, Y, and the REEs. We can use this information to distinguish primary zones of calcite from those that have been altered (see Section 6). Elements, or elemental ratios such as Ba/Ca, can be used to distinguish alteration zones or secondary material (e.g. a detrital component). For example, in meteoric carbonates, high Th is commonly attributed to detrital matter. The production of trace element maps rapidly produces extra information that can be related to any later age determination, facilitating the relating of the age to a specific growth event, i.e. the petrochronological approach (i.e. Kylander-Clark et al., 2013; Engi et al., 2017).

An alternative approach is to produce maps that generate U-Pb data directly (see Section 6.2). These have obvious utility in determining suitable domains of calcite; however, for common-lead bearing minerals they can be difficult to interpret by visual inspection. Pb-Pb or Pb-U isotope maps can be created with ease; however, because of the inherent inclusion of common lead, more useful is a map of common lead-corrected $^{206}Pb/^{238}U$ ages or ratios. Common lead-corrected age maps require: 1) precise knowledge of the initial lead

composition (or upper intercept in Tera-Wasserburg space); and 2) knowledge that the initial Pb composition is homogeneous across the mapped region, something that is not always the case (see Section 7.2). However, with the recent advent of more advanced data processing software, such as the Monocle plug-in for Iolite (Petrus et al., 2017), complex age determination from maps is becoming more amenable (see Section 6.2). The caveat with such data processing packages is that non-related domains defining a single age with a good precision can potentially be selected with subjectivity, and without relation to actual geological/mineralogical process. For this reason, we suggest that it is imperative that users relate domains they have selected for U-Pb age determination to specific mineralogical domains that can be identified independently with other means, whether these be entire crystals, domains of crystals, growth bands, or specific veinlets. As suggested by Drost et al. (2018), who demonstrate the method for carbonate sediments, it is also useful to compare conventional spot ablation analyses with the map-generated dates to verify the accuracy of the latter.

5. Analytical Protocol

The LA-ICP-MS method for carbonate follows a typical sample-standard bracketing approach using a matrix-matched reference material, i.e. as for other silicate or phosphate minerals (e.g. zircon, monazite, titanite, rutile, apatite, allanite), with only minor modifications. Similarly, uncertainty propagation and data reporting should follow the community-based guidelines for zircon of Horstwood et al. (2016). Details on the LA-ICP-MS method for carbonate adopted by three major laboratories taking a similar approach are provided in Roberts & Walker (2016) and Drake et al. (2017) for the British Geological Survey laboratory (Nottingham, UK); Ring & Gerdes (2016) and Methner et al. (2016) for Goethe-Universität (Frankfurt, Germany), and Nuriel et al., (2017, 2019) for University of California Santa Barbara (Santa Barbara, USA). Ablation spot sizes are typically larger than for silicate/phosphate minerals, generally >40 µm and often >100 µm, and fluences are also often high (>4 J/cm$^{2)}$. As with all U-(Th)-Pb LA-ICP-MS geochronology, we advocate the use of consistent ablation parameters between samples and reference materials.

There are two key points of the method we feel are worth highlighting that differ from ‘standard’ methods based on silicate minerals such as zircon. Firstly, the heterogeneous nature of the Pb isotope composition of matrix-matched, i.e. calcite/dolomite, minerals (due

to variable common Pb incorporation), means that normalisation of the Pb-Pb isotope ratios is currently achieved using a synthetic glass rather than a carbonate, typically NIST612 or NIST614. At present, there is no evidence to suggest that the Pb/Pb mass bias is variable across different matrices. Secondly, calculation of the reproducibility of the primary and secondary matrix-matched reference materials, which is for uncertainty propagation (Horstwood et al., 2016) and determination of the true method accuracy and precision, is hindered by the fact that the carbonate reference materials currently employed have U/Pb heterogeneity that is equal to or much larger than the analytical uncertainties (Roberts et al., 2017). This means there will typically be a significant excess variance of the reference material U/Pb isotope measurements in any one session (including after correction for common lead), which does not describe the reproducibility of the analytical system but instead reflects the natural variation in the reference material. If propagated onto the sample data-point uncertainties as a within-session excess variance as recommended for zircon in Horstwood et al (2016), these data point uncertainties will be overestimated, masking any smaller-scale real geological scatter in the sample isochron and resulting in ages with erroneously high precision. For this reason, it is suggested that calculation of the session-based reproducibility is best estimated using a more homogenous material such as NIST glass or zircon. However, it should be noted that through this practice results can only be compared in a relative sense within session, or between sessions if validation materials are compiled and used. To compare data in an absolute sense, i.e. to assign an age and total uncertainty to a material for comparison between laboratories and/or with other methods, the uncertainty from the primary reference material must be included to reflect the accuracy with which the matrix-matched normalisation is known. In this way, the uncertainty of the primary reference material constitutes a limiting uncertainty on any sample age. Improved reference materials with less scatter around the U/Pb isochron are therefore a pre-requisite for improving this method.

6. Generating U-Pb data and interpreting ages

Generating ages and relating these to geological processes requires the marriage of spatially-resolved variations in composition (elemental and isotopic) and U-Pb isotopic concentrations. In this section, we present several case studies to highlight how the integration of compositional image-based data with U-Pb data can be used to interpret and refine age data. First we present the ‘standard’ approach, which used independent imagery

and analysis to target, refine, and interpret the U-Pb analyses that are based on static spot ablations; this is the same concept as using CL imagery to help interpret zircon dates. A second approach (age mapping) is to use mapping tools not just to image the sample and its composition, but to extract age data from the map itself (Petrus et al., 2017; Drost et al., 2018).

6.1. Image-guided dating

The aim of most dating studies is to constrain the timing of primary calcite formation rather than subsequent secondary alteration. Trace element mapping using LA-ICP-MS is a particularly useful tool to assist with identification of growth zoning, particularly on the scale of mm- to cm-sized chips. Figures 7a and 7b show examples of vein-fill calcite where uranium zonation can be compared to other major and trace elements. The trace element mapping reveals large variation in trace element contents across the directions of growth, interpretable as changing metal/Ca ratios in the mineralising fluids (e.g. Drake et al., 2014). The trace element zonation in both of these samples can be traced with the optically visible growth zonation, indicating its primary nature. Sample TJN-0-1 (Figure 7a) was presented in Roberts & Walker (2016), and we have re-dated it here locating spots in three separate areas with different uranium concentration. The dates all overlap (Figure 7a), but the precision of the dates is controlled by the amount of radiogenic to common lead, which broadly correlates with the U concentration of the sample and where the traverse was located. For this sample, the trace elements are low, including the Mn content, meaning the entire sample appears dark in cold-stage CL. Therefore, elemental mapping with LA-ICP-MS is one of the few techniques that can be used to characterise the elemental zonation in such samples.

Sample TJN-6-1 (Figure 7b) is a single large crystal, with a rim of zeolite. Trace element mapping reveals a strong correlation between most elements, again, representing the primary growth zonation. High Mn and V ‘fingers’ intersect the growth zonation, and are visible optically. We interpret these as pathways of secondary alteration. Given that the vein exhibits vuggy textures, it is possible that fluids have precipitated or altered the original calcite much later than the original period of calcite precipitation. Trace element mapping allows us to visualise and fingerprint these alteration zones, and avoid or remove them from analyses used for dating. A benefit to this approach is that the maps can then be used to

estimate the trace metal contents of the mineralising fluids, which in turn provides information about rock-water interaction and the redox conditions, for example. These maps also demonstrate that no measurable diffusion of trace elements across the calcite crystals has occurred over a significant time span, as the distribution is interpreted as a primary feature.

Alteration zones can sometimes be observed visually, without the need for imaging techniques, as demonstrated by the vein sample in Figure 7c. In this particular sample, the CL emission was rather dark, limiting its use for distinguishing the altered and non-altered parts of the vein. Trace element mapping however, clearly distinguishes a region of alteration running across the vein that is characterised by enrichment and depletion on trace and major elements (e.g. low Mg, high La, Mn and Pb). Screening data from this sample, comprising randomly located spot traverses across the vein, are presented in Figure 7c. The data have a large array of common to radiogenic Pb compositions, with significant scatter including several data with low U/Pb and Pb/Pb ratios. The U-Pb data are compatible with open-system behaviour and/or mixed age domains. Placing spots away from the altered region, and within a region with high uranium, yields a more robust regression that we interpret as a primary date of calcite formation.

In the final example (Figure 7d), the only mapped elements were U and Pb, but the sample was also imaged using CCI. Both the elemental maps and CCI image show laminations that are interpreted as growth zonation, and a reflection of the primary distribution of trace elements (U and Pb in this case). Faintly visible on the CCI are thin veinlets that cross-cut the growth bands. On the elemental maps, these are clearly distinguished as regions of Pb enrichment and U depletion, suggesting that Pb-rich fluids have percolated through this fracture-fill calcite. Since the spots that lie on the alteration pathways have high Pb counts, the age data were culled based on Pb concentration (>300 ppb Pb removed). This approach reduced the scatter in the regression, providing a more precise age, presumably through the removal of data that reflect variable common lead compositions.

Insert Figure 7 here:

6.2. Age mapping of vein-fill carbonates

An alternative approach to using elemental maps to ‘manually’ locate spots or refine spot data, is to generate a combined elemental and U-Pb isotopic 2D dataset (i.e. map); the benefit of this method is that software tools can be used to both discriminate specific isotopic data based upon chosen criteria, and also to show regions within these pooled datasets that have similar compositional characteristics. Iolite (Paton et al., 2011) is one of the most commonly used data reduction tools for both U-Pb isotopic data (Paton et al., 2010), and for generation of elemental 2D maps. Monocle is a software plug-in for Iolite that allows the user to generate maps of isotopic and elemental data (Petrus et al., 2017), and to define and extract regions of pooled compositional data, including those used for age calculations. Drost et al. (2018) demonstrated the efficacy of the software for dating carbonate sediments, whereby features such as bioclasts and detrital components are removed. For a detailed explanation of the protocol, see Drost et al. (2018). In brief, each pixel of the elemental and isotope ratio maps corresponds to one duty cycle of the ICP-MS. First, pixels are removed, using user-defined selection criteria that are believed to be related to alteration, secondary material, or a younger or older carbonate generation. This is usually conducted after an initial inspection of the mapping data combined with prior imaging and petrography; however, the screening can also employ an iterative approach after generation of initial U-Pb isochrons. After this screening/filtering, the remaining data are pooled into a number of pseudo-analyses (each corresponding to the same number of pixels) based on a suitable isotope ratio, such as $^{238}U/^{208}Pb$ or $^{235}U/^{207}Pb$. The pooling is achieved using an empirical cumulative distribution function (ECDF) to maximise the spread in U/Pb ratios, and an appropriate number of pixels to produce a reasonable population of data, for example twenty to forty data-points. Here, we present examples of this approach applied to vein-filling calcite.

Figure 8 shows an example of a vein cross-cutting a sedimentary host-rock, with clear zonation within the vein. Since it is a syntaxial vein (crystals growing from the wall rock to the centre), this zonation probably represents changing fluid chemistry as the calcite crystals were precipitating. However, it could represent multiple generations of calcite precipitation. Criteria were selected for filtering of the data to highlight the outer regions of the vein; Rb < 0.05 ppm, Th < 0.01 ppm, and Sr < 400 ppm. The U-Pb data were then filtered to remove data with low U and Pb signals, since no initial rejection of data based on detection limit was conducted using this data reduction method; criteria for acceptance

were ^{238}U > 500 cps, and $^{207}Pb/^{206}Pb$ < 1.5. The remaining data produce a robust isochron with a lower intercept date of 61.0 ± 1.7 Ma (MSWD = 1.12; 21 pooled analyses). This date overlaps that previously obtained using spot analyses that were derived from the entire width of the vein (59.5 ± 1.7 Ma; Beaudoin et al., 2018).

Insert Figure 8 here:

To demonstrate image-based dating on another complex sample, we re-dated the vein presented in Figure 7c (NR1511). This vein features visible textures and chemistry associated with alteration. The mapped region (see Figure 9) is entirely within the vein (no host rock). High concentrations in several elements (e.g. Cu, Rb, Sr, Ba and Pb) reflect veinlets that can be seen optically as a yellow altered region. The remaining portion of the vein varies in U content, which likely represents chemical zonation across the coarse sparry calcite growth. A fairly robust isochron (MSWD = 2.0) was obtained after filtering of the data for the clearly altered regions, cleaning up the U-Pb data to remove low U and Pb signals, and pooling the data based on $^{207}Pb/^{235}U$. The criteria for acceptance were: Cu < 0.2 ppm, Ba < 10 ppm, Rb < 0.01 ppm, and ^{238}U < 10000 cps (for removal of alteration), and ^{238}U > 500 cps, $^{207}Pb/^{206}Pb$ > 0.15 < 1.5, and $^{206}Pb/^{208}Pb$ > 0.1 < 10 (for 'cleaning up' the U-Pb data). These data yielded a date of 283.1 ± 9.4 Ma, which overlaps that obtained from spot analyses and manual location of the spot data based on prior LA-ICP-MS mapping (286 ± 12 Ma; see Figure 7c).

Insert Figure 9 here:

7. Limitations

7.1. Isotopic composition of common lead

Carbonates nearly always take up some amount of lead during their formation, referred to as 'common' or initial lead. Contamination during handling (i.e. during cutting and polishing) or from recent exposure to the environment will have a modern isotopic composition of common lead, i.e. approximating the Stacey & Kramers (1975) model for terrestrial lead composition at present-day, roughly $^{207}Pb/^{206}Pb = 0.84$. Distinguishing between such contamination and the common lead incorporated during formation can be difficult. Well behaved U-Pb isotopic systematics in a carbonate sample should yield a single mixing line

between the common and radiogenic end-members, and ideally will have enough spread in U/Pb ratios to yield a precise regression with low uncertainties at both the lower (radiogenic lead) and upper (common lead) intercepts. However, many samples will exhibit a lack of spread in U/Pb ratios, or will be dominated by radiogenic compositions (e.g. Figure 4f). Although a best-fit line may be calculated for such data, the slope, and thus age, may be inaccurate. Thus, it is useful for such samples to have an estimation of the common lead composition through other means, such as from nearby cogenetic samples formed at the same age, or from different minerals also believed to have been formed at the same age.

For some mineral chronometers, such as the phosphate mineral monazite, it is common to use an estimate of the common lead composition based on the Stacey and Kramers (1975) model (e.g. Palin et al., 2013; Regis et al., 2016). In our experience, this is an acceptable approach because from a number of different studies, we find that the common lead composition determined from other minerals (i.e. feldspar, biotite, apatite) overlaps the Stacey and Kramers (1975) composition (e.g. Stübner et al., 2014; Warren et al., 2014). For carbonate however, we find this is not always such a suitable approach. Our experience, particularly from fracture-fill, but also evident in diagenetic and sedimentary carbonates, is that common lead compositions are often more radiogenic (lower $^{207}Pb/^{206}Pb$ ratios) than those predicted by the terrestrial lead model (Stacey and Kramers, 1975) for the age of carbonate crystallisation. This situation can occur if the carbonate has incorporated unsupported radiogenic lead during its formation. This most readily occurs by incorporation of radiogenic lead that is derived from an ancient source, i.e. lead produced by uranium decay in a closed system for a long time, but which is decoupled from its parent uranium before being incorporated into the measured carbonate.

We have compiled sample data with robust U-Pb regressions from the BGS laboratory (both published and unpublished), and presented these as a compilation of common lead intercepts ($^{207}Pb/^{206}Pb$). The data are split into fracture-fill and diagenetic samples, and represent different host lithologies, different ages (dominated by Cretaceous to Miocene), and different geological regions. It is clear that for many samples in this compilation, anchoring at a value close to the terrestrial lead model composition for Phanerozoic ages, i.e. $^{207}Pb/^{206}Pb \sim 0.84$, will lead to calculated ages older than the true age due to steepening of the regression. The importance of the common lead composition in providing constraints on a calculated age will depend on the amount of measured radiogenic lead in a

given sample; samples dominated by common lead and lacking in radiogenic lead will need a well-defined array to produce a confident lower intercept. We find that within individual vein samples, the apparent composition of the common lead end-member can vary, limiting the precision of the regression and derived age. For speleothems, Woodhead et al. (2012) demonstrate that most samples analysed in their lab yield common lead compositions overlapping Stacy and Kramers (1975), and thus their ages are largely insensitive to the common lead compositions. This likely reflects the fact that they are precipitated from meteoric water that incorporates modern lead derived from a regional upper crustal lead composition.

The highly radiogenic initial lead values ($^{207}Pb/^{206}Pb < \sim 0.75$) recorded in our compilation are mostly from two settings, young fractures in Proterozoic crystalline crust of Sweden (n= 10), and young fractures in the Bighorn Basin that overlies Archaean basement (n=24). In both cases, lead leached from the bulk-rock, although ancient, is not radiogenic enough to produce the measured values. Instead, leaching of unsupported radiogenic lead from uraniferous minerals (i.e. high μ) is required (e.g. titanite, allanite, monazite, xenotime and zircon) as a causative mechanism. Radiogenic lead is in fact a well-known widespread feature found in ore deposits across Sweden (e.g. Johansson & Rickard, 1984; Romer & Wright, 1993).

Insert Figure 10 here:

An additional complexity in interpreting carbonate U-Pb data, is that fine-scale variability in initial lead compositions may exist. This is because the fluids involved in carbonate precipitation may vary on very short timescales, with varying fluid-rock interaction leading to different Pb components being leached into the fluids. The time-scale of varying fluid involvement may be much shorter than the resolution of the U-Pb data, such that data with variable initial lead compositions may not be resolvably different in age, and hence, will merely lead to increased scatter on the U-Pb isochron. Heterogeneous initial lead compositions can be seen in an example of sandstone-hosted vein material from the Moab fault, southeast Utah (Figure 11). U-Pb data were obtained from different sections of the vein material formed along different orientations. The data exhibit a high level of common/initial lead, with limited spread in radiogenic lead contents, but still forming a

765 scattered regression to a lower intercept value. Using different colours to discriminate
766 different sections of vein, it is clear that they have subtly different initial lead compositions,
767 as indicated by the upper intercept ($^{207}Pb/^{206}Pb$ value) of the data arrays. These lead
768 compositions are more radiogenic from that predicted by the Stacey & Kramers (1975)
769 terrestrial composition. The existence of variable Pb compositions on small length-scales
770 (<1 mm) means that careful attention is required to interpret complex data. However, the
771 spatial resolution of LA-ICP-MS means that these details can potentially be teased out.
772
773 *Insert Figure 11 here:*
774
775 In summary, vein-filling, diagenetic and hydrothermal carbonates often do not exhibit Stacy
776 & Kramers (1975) model Pb compositions for their assumed age, but typically yield more
777 radiogenic compositions. This means that regressions anchored with assumed common
778 lead compositions are susceptible to inaccuracy. Mixed common lead compositions in
779 samples hampers derivation of single age regressions, implying multiple fluid sources.
780 Mixed ages and atypical lead compositions can also make age mapping problematic.
781
782 7.2. Dating young material – dealing with disequilibria
783 As described in Section 3, the younger the age of the sample analysed, the lower the
784 potential for precise and accurate age determination due to the lack of radiogenic ingrowth
785 of lead. However, young carbonates are a high priority in many applications, because they
786 can date events more relevant to the Earth system at present, and because U-Pb can
787 extend the age range of sample suites or study areas where U-Th age dating is also
788 feasible. For example, records of environmental change in deep time require the dating of
789 speleothems that are older than 500 ka (see Woodhead et al., 2012, 2019), and dating of
790 veins that record seismic cycles extending beyond 500 ka (see Uysal et al., 2011; Williams
791 et al., 2017) can provide constraints on earthquakes and other hazards associated with
792 subsurface fractures. These particular applications are likely to require high levels of
793 precision, i.e. for the Quaternary, of much less than ± 100 ka, and potentially even less than
794 ± 10 ka or < 1000 years for the Holocene. Achieving such precision requires very high U to
795 achieve abundant radiogenic lead and higher μ values (see Figure 3).
796

A major issue for accurate dating of young samples (i.e. <10 Ma) is the potential effect of initial daughter isotope disequilibrium within the uranium decay chains. The simplest form of the U-Pb and Pb-Pb age equations, often used for older samples, assume that all long-lived daughter isotopes in the U decay chain are initially present in secular equilibrium. Both the U decay series contain long-lived daughter isotopes, including ^{234}U ($t_{½}$ = 245 ka), ^{230}Th ($t_{½}$ = 76 ka), and ^{226}Ra ($t_{½}$ = 1.6 ka) in the ^{238}U decay chain, and ^{231}Pa ($t_{½}$ = 34 ka) in the ^{235}U decay chain. Of these, ^{234}U has the longest half-life and therefore the largest potential effect on U-Pb dates. The excess initial ^{234}U often observed in natural waters will lead to generation of unsupported ^{206}Pb. If uncorrected, excess initial ^{234}U produces overestimated $^{206}Pb/^{238}U$ and lower intercept dates. An excess of the other intermediate daughter products, like ^{230}Th, relative to secular equilibrium will bias the age with a smaller magnitude but in the same direction, whereas a deficit will result in dates that are too young.

Carbonates are commonly precipitated from fluids containing $^{234}U/^{238}U$ out of secular equilibrium. Thus, this initial disequilibrium must be considered in any age determination. Age corrections for initial U daughter deficits are at maximum ~1.44 times the half-life of the daughter isotope for zero initial abundance. But for initial excesses, the age difference can be many times larger. For most older samples dated by U-Pb, the effect of disequilibrium is deemed to be insignificant compared to larger measurement uncertainties. For this reason, initial disequilibrium has thus far not been mentioned in any publication concerning LA-ICP-MS U-Pb dating except for those dealing with young speleothems (e.g. Hopley et al., 2019). However, here we demonstrate that initial disequilibrium may be a very significant cause of uncertainty for carbonates precipitated from groundwater and other crustal fluids, and not just for very young (<1 Ma) samples.

In young samples, particularly those within the range of U-Th geochronology (<600 ka), the initial $^{234}U/^{238}U$ ratio ($^{234}U/^{238}U_0$) can be estimated based on the combination of the present-day measured $^{234}U/^{238}U$ ($^{234}U/^{238}U_{now}$), and either the measured $^{230}Th/^{238}U$ or the estimated date of formation. The robustness of this estimate is highly dependent on the precision and accuracy at which the isotope ratio(s) can be measured (the atom ratio is very small, making high precision measurement >1‰ difficult). In addition, if the offset between $^{234}U/^{238}U_{now}$ and secular equilibrium is small, then the measurement may overlap secular

equilibrium within uncertainty. For this reason, the highest precision possible is a necessary target for any disequilibrium correction measurement.

For older samples (i.e. those older than about four times the half-life of ^{234}U), and/or those with only a small degree of initial disequilibrium, $^{234}U/^{238}U_{now}$ is likely to have reached secular equilibrium. This means that $^{234}U/^{238}U_0$ cannot be estimated from the measured data alone. One approach to alleviate this problem is to take known initial ratios from younger samples (<600 ka) formed in approximately the same geologic setting, and apply these corrections to the older samples from the same setting (e.g. Woodhead et al., 2006, 2019). This approach is only applicable if the geological environment is well known and the hydrological system believed to be relatively stable.

There are various causes of ^{234}U excess in fluid-mineral systems, which have been studied at length (e.g. Osmond & Cowart, 1992, 2000; Porcelli & Swarzenski, 2003; Suksi et al., 2006). In summary, ^{234}U is generated from α decay of ^{238}U, and may preferentially be increased in the fluid state during mineral-fluid interaction due to oxidation state and valence differences between the U species (e.g. Suksi et al., 2006). Uranium activity ratios record information on the redox state of fluids, the source of uranium in the fluids, and potentially the timing of uranium residence in the fluid; therefore, they have long been a focus of groundwater studies (e.g. Osmond et al., 1968; Osmond & Cowart, 2000; Porcelli & Swarzenski, 2003). Of general interest here, is whether carbonates precipitated from different geological settings are likely to have significant ^{234}U excess such that any measured $^{238}U/^{206}Pb$ dates will be inaccurate.

Cave drip-water that generates speleothem deposits typically has excess ^{234}U relative to secular equilibrium, although sometimes ^{234}U is depleted. Overall, most cave systems have initial activity ratios that are not grossly offset from secular equilibrium. This means that an uncertainty limit can be placed on such carbonates with reasonable confidence. Disequilbrium corrections will significantly affect age estimates with high precision, but not the low precision estimates that typically characterise LA-ICP-MS dates. For example, Woodhead et al. (2019) used an estimate of 1.0 ± 0.3 for $^{234}U/^{238}U_0$ in their study of speleothems from the Nullarbor plain, Australia, and this had negligible impact on the resultant compilation of U-Pb dates. Hopley et al. (2019) estimated a range of $^{234}U/^{238}U_0$ = 1.26 to 2.99 for the ‘Cradle of Humankind’ in South Africa, with a mean of 1.9, and

discussed a resulting potential age range of 5.8 to 4.8 Ma. A known excursion from 'typical' activity ratios is the Transvaal Dolomite Aquifer, also in South Africa. Speleothem deposits in cave systems that interacted with water from this aquifer have anomalously high U activity ratios ranging from ca. 2 to 12 (Kronfeld et al., 1994). This well-known occurrence highlights that speleothem deposits could arise from fluids with variable and anomalous activity ratios, and thus that attention must be given to accurately estimating the $^{234}U/^{238}U_0$ when dating such deposits.

Unfortunately, activity ratio data that is relevant to hydrothermal and other vein-filling carbonates is sparse and potentially more variable. Carbonates precipitated in the shallow crust may arise from percolating groundwater, seawater, deep brines, formation waters, or a mixture of these sources. We can use existing data on these fluid sources to make an initial estimate of what range may exist in terrestrial carbonates. Groundwater is well known to have highly variable and significant ^{234}U excess (e.g. Osmond and Cowart, 1976). Figure 12 shows a compilation of $^{234}U/^{238}U$ activity ratios taken from a range of literature sources (see supplementary file for sources). The population of data for groundwater (Figure 12a), mostly shallow, but including some saline and deeper samples, has a median activity ratio of 2.25, and is skewed towards higher values, with a significant tail up to ~11. Data from hydrothermal fluids and deep brines are less abundant in the literature, but can be estimated from young carbonates precipitated in travertines and hydrothermal veins. The compilation shown in Figure 12b is dominated by samples from Turkey and surrounding regions. It has a median of 1.41, and is right-skewed with a tail ranging up to ~8 and only a few higher values.

Insert Figure 12 here:

The compilations in Figure 12 are somewhat alarming, as they suggest that vein-filling carbonates have a high likelihood of having activity ratios out of secular equilibrium (where $^{234}U/^{238}U$ = ~1). The compilations shown are biased by sampling, so uncertainties on the range of activity ratios should not be based on these compilations. However, a very conservative view would be that shallow groundwater $^{234}U/^{238}U$ activity ratios average closer to ~2 than they do to ~1; hydrothermal waters average closer to ~1.5; and permissible values may be extremely out of secular equilibrium at >10. The data reveal that

precise age estimates of young carbonates derived from crustal fluids are going to be severely hampered by a lack of knowledge of the U activity ratios.

To demonstrate the effect of initial activity ratios out of secular equilibrium, we have modelled synthetic data in Figure 13. This figure shows curves representing samples of ten different ages, which would range from 500 ka to 9 Ma if $^{234}U/^{238}U_0$ was in secular equilibrium (~1) during formation. The true age of the samples get younger as $^{234}U/^{238}U_0$ increases. The effect does not decrease in significance as we look at older ages, i.e. the age offset on a sample with a measured age of 8 Ma is similar to that on a sample of 4 Ma. The curves are shown on a log scale, because in many systems, the variation in activity ratio is going to vary a small amount, close to secular equilibrium (~1). For example, in the Nullarbor plain cave systems, the variation is likely to be within 30% of 1 (Woodhead et al., 2019). Systems with large variations in initial activity ratios, for example some hydrothermal systems, would lead to a large uncertainty on the obtained dates. Ignoring the effect of the likely ^{234}U excess in vein-filling carbonates is likely to lead to significant inaccuracy of dates by 10s of %, in general by overestimating the age. Considering the impact that unconstrained initial $^{234}U/^{238}U$ ratios have on young dates leads to significant (> 10%) uncertainties.

Insert Figure 13 here:

So far, the discussion has involved the uncertainties surrounding excess/deficient ^{234}U during calcite growth. However, there are several other intermediate daughter products in the uranium decay chains that can pose problems for the accuracy of measured ages; see Richards et al. (1998) and Woodhead et al. (2006) for previous discussion of these. The isotope ^{230}Th is a potential consideration in the accuracy of ^{238}U-^{206}Pb ages. In general, most speleothem-dating studies assume no initial ^{230}Th in the system, as Th is very insoluble in water compared to U. Any excess initial ^{230}Th during formation would also result in artificially old measured ages. ^{231}Pa is another daughter product in the decay chain, which again, is considered very insoluble, and does not form part of the disequilibrium corrections at present. ^{226}Ra, another intermediate product, may co-precipitate with U, but its short half-life of 1.6 ka means it is likely to have little impact on U-Pb ages (Richards et al., 1998). A final concern is the gas ^{222}Rn, as this may be lost from the system by diffusive

processes. A study into the effect of this showed negligible impact on the ^{238}U-^{206}Pb ages of a Quaternary speleothem (Richards et al., 1998).

Although the effects of disequilibrium in these shorter-lived intermediate daughter products is considered to be minor, and likely within the uncertainty of measured LA-ICP-MS U-Pb dates, it is worth noting that hydrological systems outside of those concerning speleothems and meteoric water have not been explored. Most of the issues presented here, particularly the excess ^{234}U problem, are part of the ^{238}U decay chain, and thus have implications for $^{238}U/^{206}Pb$ and lower intercept ages. The ^{235}U decay chain has different intermediate daughter products, and thus measured $^{235}U/^{207}Pb$ and lower intercept ages will be affected by a different set of processes. The problem of excess ^{234}U is alleviated if ^{235}U-^{207}Pb ages can be used instead of ^{238}U-^{206}Pb ages. However, there have been few attempts to utilise ^{235}U-^{207}Pb dates (e.g. Hopley et al., 2019) because the low abundances of these isotopes in comparison to ^{238}U and ^{206}Pb are major limitations on the uncertainty of the measurements. Engel et al. (2019) have provided a solution that will potentially increase the accuracy of age estimates for speleothems, utilising the ^{235}U decay chain, as well as using ^{208}Pb in place of ^{204}Pb as the initial lead composition. This approach is based on ID, and it is unclear how effective it will be for LA-ICP-MS dating, given that ^{204}Pb is difficult to measure at high precision.

In summary, initial disequilibrium is clearly a major issue for the accuracy of U-Pb dating of carbonates. The effect is significant for material of any age, but as we get to older carbonates, the analytical uncertainty contributions will begin to swamp the uncertainties surrounding disequilibrium. For dating of Neogene-Quaternary carbonates, prior knowledge of likely activity ratios (e.g. by measuring younger or present-day values of the precipitating fluid, and inferring no change back in time) is critical for precise and accurate dates. The variation in hydrothermal systems that mix meteoric water with older brines is likely to be large in terms of the degree of ^{234}U excess. More information is needed to further understand what sort of values can be expected in different systems and different settings. From our preliminary compilation, it is apparent that ^{234}U excess is the norm, rather than the exception. For now, the absolute values and uncertainties on young dates (late Neogene to Quaternary) with no estimation of the initial disequilibria should be treated with caution.

7.3. Dating old material – dealing with a potentially open system

Many early carbonate dating studies were attempted on very old material, i.e. Proterozoic and Archaean (e.g. Moorbath et al., 1987; Jahn, 1998; Taylor and Kalsbeek, 1990; Whitehouse and Russell, 1997); these mostly utilised Pb-Pb dating. A major issue of the Pb-Pb method, is that Pb contents of crustal fluids are much higher than that of the primary carbonates, and therefore, even small amounts of fluid-related alteration can dominate the measured Pb-Pb composition and lead to an age that is not representative of primary carbonate precipitation (e.g. Sumner & Bowring, 1996). Although there have been a handful of studies dating old carbonate material since the 1990s (e.g. Ray et al., 2003; Sarangi et al., 2004; Babinski et al., 2007; Fairey et al., 2013), Pb-Pb and U-Pb dating of Precambrian material have become rarely used techniques. This is presumably due to the difficulty in obtaining meaningful primary ages of old material. The dominant reason for this difficulty can generally be distilled down to open-system behaviour, i.e. dating material that has remained a closed isotopic system since its formation is increasingly difficult with increasingly older material. This is simply because thermal- and/or fluid-induced mobility of parent and daughter isotopes becomes increasingly likely if the material has been exposed to multiple deformation-, burial-, uplift-, glaciation-, weathering- or fracture-related events.

Early studies documented various transformative processes and their impact on Pb-Pb/U-Pb isotope systematics, e.g. fluid infiltration in limestone (Smith et al., 1991), diagenetic change from aragonite to calcite (Jones et al., 1995), and resetting of Pb isotope signatures during metamorphism (Russell et al., 1996; Whitehouse and Russell, 1997; Babinski et al., 1999). In general, the existence of some form of open-system behaviour within a given dataset has only been recognised through the isotopic data themselves, not through an independent dataset. This is simply achieved by assessing the robustness of the Pb-Pb or U-Pb data array with mathematical means, e.g. using the MSWD value, and explaining analytical scatter outside of a robust array as due to open system behaviour. With *in situ* methods, the approaches that we have described in Section 5 may allow for some independent removal of data that pertains to open-system behaviour, leaving a dataset that corresponds to a closed system.

A method that has been utilised to screen for altered samples in whole-rock geochemistry, is to test for effects of modern weathering using $^{234}U/^{238}U$ ratios (Albut et al., 2019). Ancient samples should have measured $^{234}U/^{238}U$ activity ratios in secular equilibrium, and

997 departure from this in a measured sample would imply a more recent addition or subtraction
998 of ^{234}U through weathering processes, indicating some modern fluid-rock interaction. This
999 method of sample screening has not been applied to U-Pb dating, but we suggest is worthy
1000 of investigation.
1001
1002 In Figure 4 we documented various U-Pb datasets to demonstrate the range of behaviour
1003 that is seen with natural carbonates. Here we provide some additional comments regarding
1004 open-system behaviour, first in terms of U mobility, followed by that of Pb mobility. Uranium
1005 is mobile in oxidising fluids, so U enrichment and depletion relative to Pb is assumed to be
1006 the most common cause of open-system behaviour that will occur in natural carbonates. In
1007 Tera-Wasserburg space ($^{238}U/^{206}Pb$ vs. $^{207}Pb/^{206}Pb$), U mobility will be apparent as sub-
1008 horizontal trends in the data, with movement to the right reflecting gain of ^{238}U, and
1009 movement to the left reflecting loss of ^{238}U (see Figure 14). During a period of mobility,
1010 uranium may move into a fluid-phase, such that the remaining carbonate solid remains
1011 variably depleted in ^{238}U, or, uranium may partially move from its original location to another
1012 within the measured sample volume. In the former, this can sometimes be detected from
1013 the isotopic data if a distinct departure from a robust regression is defined by a sub-
1014 horizontal array (see Figures 4d). In the latter case of uranium mobility, some domains will
1015 be depleted, whereas others will be enriched. This may be difficult to ascertain from the
1016 isotopic data alone if the mobility is pervasive through the material, because the induced
1017 scatter in the U-Pb regression (from both positive and negative movement in $^{238}U/^{206}Pb$)
1018 cannot be resolved from other causes of scatter, such as mixing between different age
1019 domains.
1020
1021 *Insert Figure 14 here:*
1022
1023 Lead can substitute for Ca in the calcite lattice, and is also insoluble in most upper crustal
1024 fluids, for these reasons, U mobility is generally considered in favour of Pb mobility. Fluid-
1025 assisted mobility of U is certainly the most likely cause of open system behaviour because
1026 of the solubility of some U species. However, at high temperatures, solid-state diffusion is
1027 also a factor for consideration. Based on experimental data, Pb diffusion in calcite is
1028 essentially slow enough to be non-existent below 300°C (when considering the composition
1029 of a grain 1 mm in diameter; Cherniak, 1997); however, at higher temperatures (>400°C),
1030 diffusion of lead is possible if encountered for long periods (> 20 Myrs). Empirical

observations of Pb (or U) diffusion in calcite are lacking. Diffusion is unlikely in the low temperature calcites that have formed the basis of most modern LA-ICP-MS dating studies; however, carbonates form in a range of higher temperature environments as well, such as alteration veins within deeply subducted crust. Understanding how the calcite U-Pb system works at medium to high-metamorphic grades may therefore become very relevant information, allowing this chronometer to be used to understand dates and rates in deep crustal environments.

7.4. Analytical limitations

At present, there is only one reference material in circulation that has been widely used and documented for the purpose of U-Pb normalisation (WC-1; Roberts et al., 2017). WC-1 has an uncertainty on its U/Pb ratio of 2.5% 2σ. Using this material for normalisation of U/Pb ratios, or for validation of the method accuracy, limits the final age uncertainty of any particular sample to ~2.5%. To improve beyond this range requires the characterisation of natural (or production and characterisation of U and Pb doped synthetic) materials, with a final U/Pb precision better than 2.5%. There is also a requirement for additional well characterised materials (i.e. those with robust U-Pb systematics and well documented ID U-Pb datasets) that can be used as secondary reference materials (i.e. those run as unknowns), for assessment of accuracy and long-term reproducibility.

Another major limitation is the nature of carbonate matrices, and the lack of quantified data on the matrix effect between different carbonate minerals and structures. Inter-element fractionation (i.e. U/Pb in this case) is one of the major limitations on the reproducibility and accuracy of laser ablation U-Pb dating. For this reason, matching matrices of the reference material with that of the sample has been standard practise in U-bearing accessory mineral geochronology. Several groups have tried to limit the effect of this issue by utilising normalisation and data reduction procedures that reduce the effect (e.g. Burn et al., 2017; Neymark et al., 2018), but regardless of the matrix used for normalisation, validation of the method should still utilise a similar matrix to the sample. Carbonates clearly have a large range of structures, even with calcite, for example, sparry to micritic, with wide-ranging crystal/grain-sizes and porosity. Nuriel et al. (2019) noted differences between the use of coarse-grained sparry reference materials to fine-grained polycrystalline reference materials, with the latter being skewed towards older ages by several percent. To move

towards better precision and accuracy of the LA-ICP-MS U-Pb method, it will be necessary to have a range of well characterised reference materials that cover variable carbonate mineralogy (e.g. aragonite, dolomite, calcite), as well as internal morphology and texture.

8. Applications of carbonate geochronology

To date, LA-ICP-MS U-Pb carbonate geochronology has been utilised for a wide range of applications. These include the dating of speleothem deposition (Hopley et al., 2019; Scardia et al., 2019; Nicholson et al., 2020), brittle deformation (Roberts & Walker, 2016; Ring & Gerdes, 2016; Goodfellow et al., 2017; Hansman et al., 2018; Parrish et al., 2018; Beaudoin et al., 2018; Nuriel et al., 2017, 2019; Smeraglia et al., 2019), hydrocarbon migration (Holdsworth et al., 2019, 2020), hydrothermal ore mineralisation (Burisch et al., 2017, 2019), hydrothermal and deep crustal fluid flow (Drake et al., 2017, 2019, 2020; Mazurek et al., 2018; Walter et al., 2018; Incerpi et al., 2019; MacDonald et al., 2019), pedogenesis (Methner et al., 2016; Liivamägi et al., 2019), ocean crust alteration (Coogan et al., 2016), diagenesis in sedimentary deposits (Li et al., 2014; Pagel et al., 2018; Mangenot et al., 2018; Godeau et al., 2018; Lawson et al., 2018) and sedimentary deposition (Drost et al., 2018). Published dates range in age from 0.6 to 548 Ma (see Figure 15), MSWDs range from 0.2 to 89 (Figure 15a), and quoted uncertainties range from 0.6 to 143 % (2s; Figure 15b). The majority of dated samples so far range from the Neogene to Jurassic, with ~50% being Oligocene or younger. Across this age range, the uncertainty is variable and uncorrelated to age or MSWD, demonstrating that the age uncertainty reflects an interplay of factors, and includes the heterogeneous nature of carbonate materials. It should be noted however, that many dates with large uncertainties or mixed results are likely unpublished, biasing this compilation towards successful samples. For example, it is possible that many unreported and failed attempts at dating samples that are Palaeozoic and older have been made. We also note that many samples have reported age uncertainties better than the WC-1 RM, indicating that the systematic uncertainties have not been fully incorporated for these dates.

Insert Figure 15 here

A major benefit of carbonate geochronology is that carbonate minerals provide an archive of data that can be linked to the age of formation. Fluid inclusions, stable isotopes (carbon

and oxygen), radiogenic isotopes (strontium), and elemental compositions all reveal insight into the fluid composition that precipitated the mineral. This combination has long been an approach within the field of palaeohydrology; however, the timing of mineralisation and hence fluid-flow has generally involved only relative estimates with large uncertainties, or the dating of phases associated with higher-temperature activity (e.g., Re-Os dating of Molybdenite). The addition of absolute chronological information is a critical step to understand the timing of fluid-flow through the crust in a range of settings, for example, within hydrocarbon-bearing basins, within ore-forming mineral systems, and within upper crustal bedrock that may be used to host anthropogenic waste/outputs (e.g. radioactive waste, storage and sequestration of CO_2).

A benefit of utilising LA-ICP-MS as a method of dating, is that the same crystals that have been dated can be measured for various other chemical proxies and signatures. Several previous studies have combined fluid inclusions and/or stable carbon and oxygen isotope analysis with LA-ICP-MS dating (e.g. Mangenot et al., 2018; Pagel et al., 2018; Goodfellow et al., 2016; Walter et al., 2018), but for most of these, it is not clear if the same volume of material, or simply the same genetic domain has been sub-sampled for both the dating as well the additional isotope analyses. Use of petrography and imaging allows for the same genetic domain to be analysed for several methods; however, there are also several approaches that allow for an overlapping analytical volume to be analysed. Dated material can be micro-drilled or -milled following laser ablation, with the powder being analysed for additional chemical information (e.g. Sr, C, O isotopes). Alternatively, thin sections or polished blocks can be analysed using a combination of in situ techniques, for example, ion microprobe measurement of stable isotope and/or elemental compositions, and laser ablation measurement of Sr isotopes, elemental compositions along with U-Pb dating. Drake et al. (2017, 2019, 2020) demonstrate the utility of combining ion microprobe stable carbon and oxygen isotope analysis with U-Pb dating to study palaeohydrology and ancient microbial activity.

In addition to traditional carbon and oxygen isotope measurements ($\delta^{13}C$ and $\delta^{18}O$), clumped isotopes ($\Delta 47$) can provide the temperature of mineral formation (e.g. Eiler, 2007). Several studies have demonstrated the combination of clumped isotope thermometry with dating (e.g. Quade et al., 2018; Mangenot et al., 2018; Lawson et al., 2017; MacDonald et al., 2019). These apply the technique to the dating of paleosols for climatic records,

diagenetic mineralisation for basin histories, and hydrothermal veins to understand crustal fluid-flow. This combination of techniques is a clear growth area with a range of applications across earth and environmental science.

Finally, carbonates also comprise a host of major and trace metals that offer further isotopic information that has yet to be fully explored, for example, stable isotopes of Ca, Zn, Fe, and Cu. Linking these with U-Pb dates from the same material could provide high resolution records of natural fractionation processes in subsurface environments.

9. Conclusions

LA-ICP-MS U-Pb carbonate geochronology has been demonstrated by this and previous studies, to offer a potentially robust technique to date the timing of carbonate mineral formation. Limitations on the technique arise from several challenges. These include the typically low U content of carbonates in many settings, the propensity for carbonate to include significant concentrations of Pb upon formation, and the ease with which fluids can alter or reprecipitate mineral growth. LA-ICP-MS being an *in situ* technique, with high spatial resolution compared to physical sampling for bulk dissolution studies, enables many of the hurdles in carbonate geochronology to be overcome.

Accurate and informative U-Pb carbonate geochronology demands careful imaging and petrographic analysis to establish a link between date and process. Various imaging techniques can be utilised prior to or after dating to aid with mineral characterisation, and with refinement and interpretation of the resulting age data. We refer to this as image-guided analysis. An alternative technique involves directly determining age data from image-based data itself, which we refer to as image-based analysis. Both techniques have their different benefits and applicability, and their efficacy depends on the instrumentation used and the type of material; for example, quadrupole ICP-MS is suited to image-based analysis, as a large element suite can be measured. Limitations on using quadrupole instrumentation are the detection limits for U and Pb when counting a large suite of elements. In contrast, multi-collector instruments can be used for image-based analysis, and have a very low detection limit, but the mass range is restricted between Hg and U, meaning that additional elements useful for understanding the U and Pb distribution cannot

be measured simultaneously. Overall, image-based analysis is only nascent in geochronology, and as such has not been fully explored.

Limitations on the accuracy of ages and their interpretation, comes from several sources. Variability in initial lead composition needs to be acknowledged when interpreting complex U-Pb data, and carbonates commonly have initial compositions that are different to that predicted by model estimates, e.g. Stacey & Kramers (1975). Disequilibrium in the U-Pb decay chains is typically only explored in very young samples (<1 Ma), but can have a potentially significant effect on the accuracy of ages throughout the Quaternary to Neogene. The variability in U isotope ratios in natural waters is a cause for concern in dating young material, and indicates that more work to understand the natural variability that can be expected in carbonate precipitates is required.

The applications of carbonate U-Pb geochronology are vast, with a key benefit to the laser ablation approach being that specific volumes of material can be analysed for several isotopic and elemental proxies and signatures, whilst also providing absolute chronological information. The LA-ICP-MS method is limited by factors that include the uncertainties on reference material isotope ratios, matrix effects and long-term reproducibility; taking these into consideration, the method is best applied to applications where age uncertainties of greater than 3-4% are of benefit. For applications where high precision (i.e. <1%) is required, such as calibration of palaeoclimate records or of evolutionary change, then follow-up analysis with ID is the only method that can potentially achieve the necessary precision. The future of the method in terms of accuracy and precision requires well characterised (by Isotope Dilution methods) reference materials covering a range of carbonate matrices. The range of studies published over the last five years (2014 to 2019) have revealed a wide array of geoscience applications that are both amenable to, and benefit from, LA-ICP-MS U-Pb carbonate geochronology.

10. Acknowledgements

The authors acknowledge the Natural Environment Research Council for National Capability funding of the National Environmental Isotope Facility. D Chew and K Drost acknowledge a Science Foundation Ireland grant (15/IA/3024) that is partly funded by the Geological Survey of Ireland and the Environmental Protection Agency, Ireland. HD

acknowledges Swedish Research Council grant (2017-05186) and Formas grant (2017-00766). NR thanks Jeremy Rushton for continued support and interest in sample petrography, Joe Emmings for help with R, and Troy Rasbury, Randy Parrish and Chris Smith for discussion and encouragement during the ‘early years’ of carbonate dating at the BGS.

11. Code/Data Availability

U-Pb data presented in Section 6 are provided in the supplementary table, along with the corresponding methods and analytical details in the supplementary text.

12. Author contribution

NR, KD, DC and AS collected the analytical data. MSAH and DC provided oversight to data collection and interpretation. AM, HD and JL assisted with sample petrography. RW, RH and JI assisted with sample collection. KD, NB, JL and RW contributed samples. NM assisted with data analysis. NR collated literature data. All authors contributed to writing the paper.

13. Competing Interests

All authors have no competing interest.

14. Special issue statement.

This article is part of the special issue “In situ carbonate U–Pb geochronology”. It is a result of the Goldschmidt conference, Barcelona, Spain, 18–23 August 2019.

15. Figures

Figure 1. Maps of uranium in vein-filling calcite from a range of geological settings showing varying styles of distribution, see text for explanation. Maximum concentration (yellow) is shown below each map; brighter = higher concentration. Maps were generated using LA-ICP-MS trace element analyses and the Iolite data reduction software. Scale bars are 1 mm.

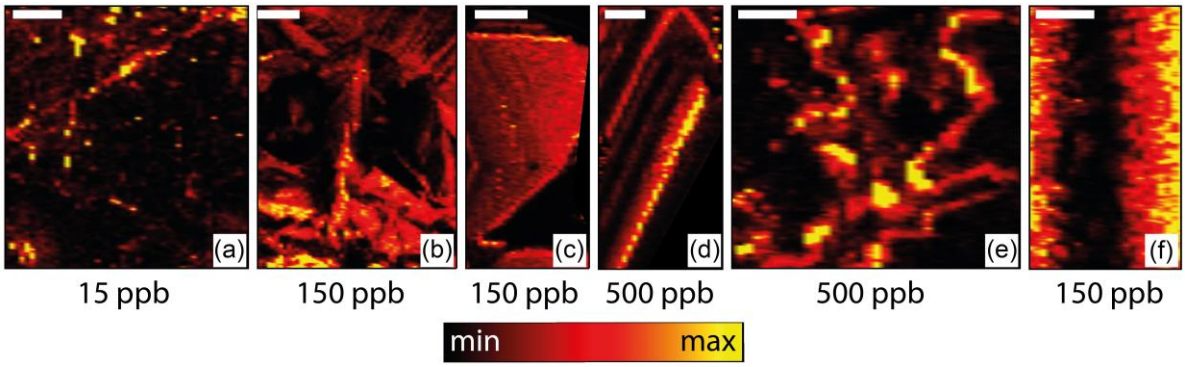

Figure 2. (a) Example Tera-Wasserburg Concordia plot demonstrating the functionality of this plot for common-lead bearing U-Pb data. (b) Schematic model of a calcite crystal with uranium zonation indicated by the colour-scale. Typical relative sample size for low U (<1 ppm) ID shown by the black squares, and LA-ICP-MS by the circles. (c) Resultant U-Pb data in Tera-Wasserburg concordia assuming constant Pb concentration across the sample, for LA-ICP-MS versus 'bulk' sampling and ID analyses, as represented by the sampling in B. The uncertainties on the datapoints are 2-3% (2s) for LA-ICP-MS and ~0.8% for ID.

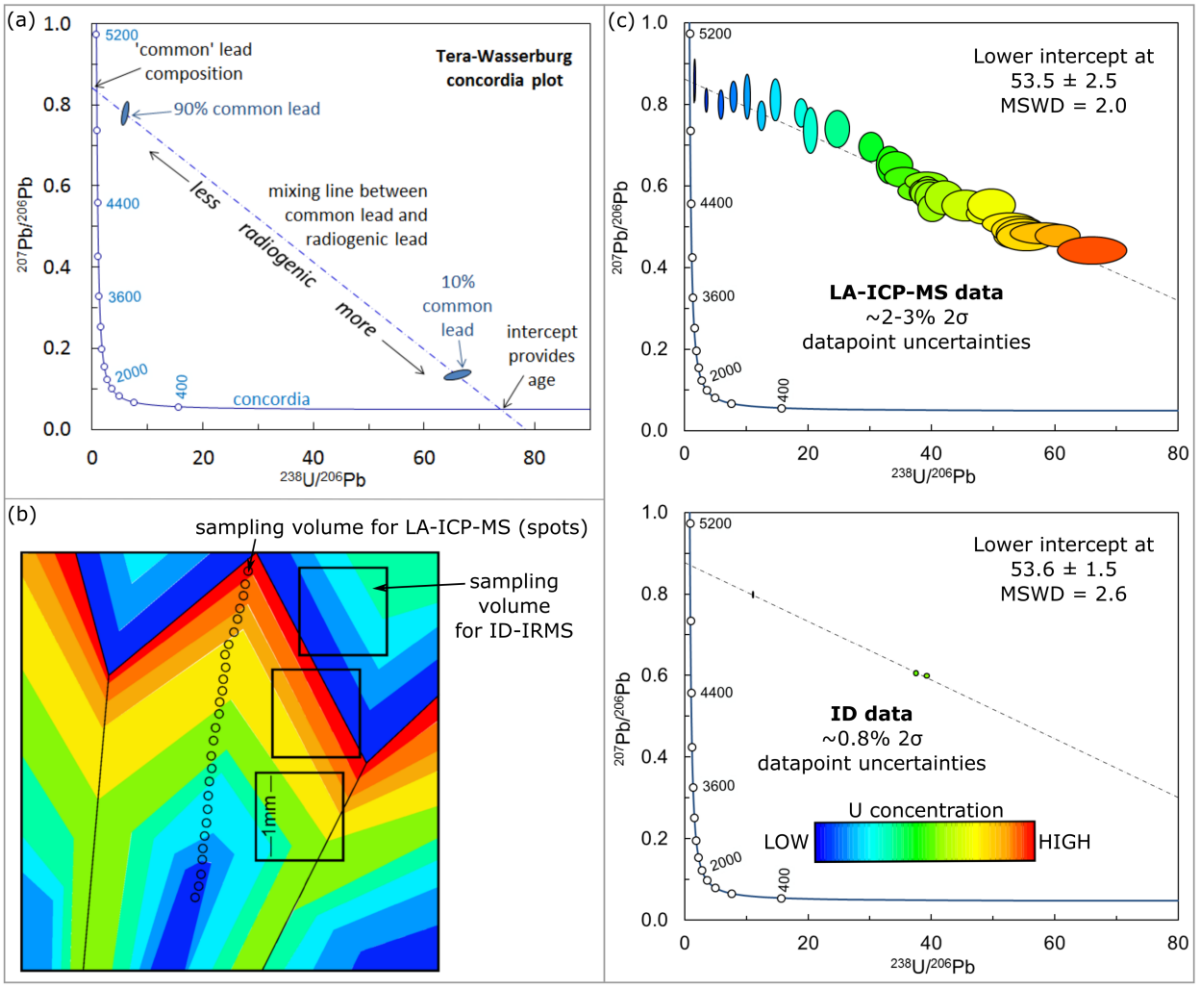

Figure 3. Tera-Wasserburg plots showing modelled regressions for samples of different age. Colour-coded spots relate to the measured isotope composition a sample would have at a given μ value (legend above). Ages of each regression in Ma are labelled adjacent to the lower intercept with concordia.

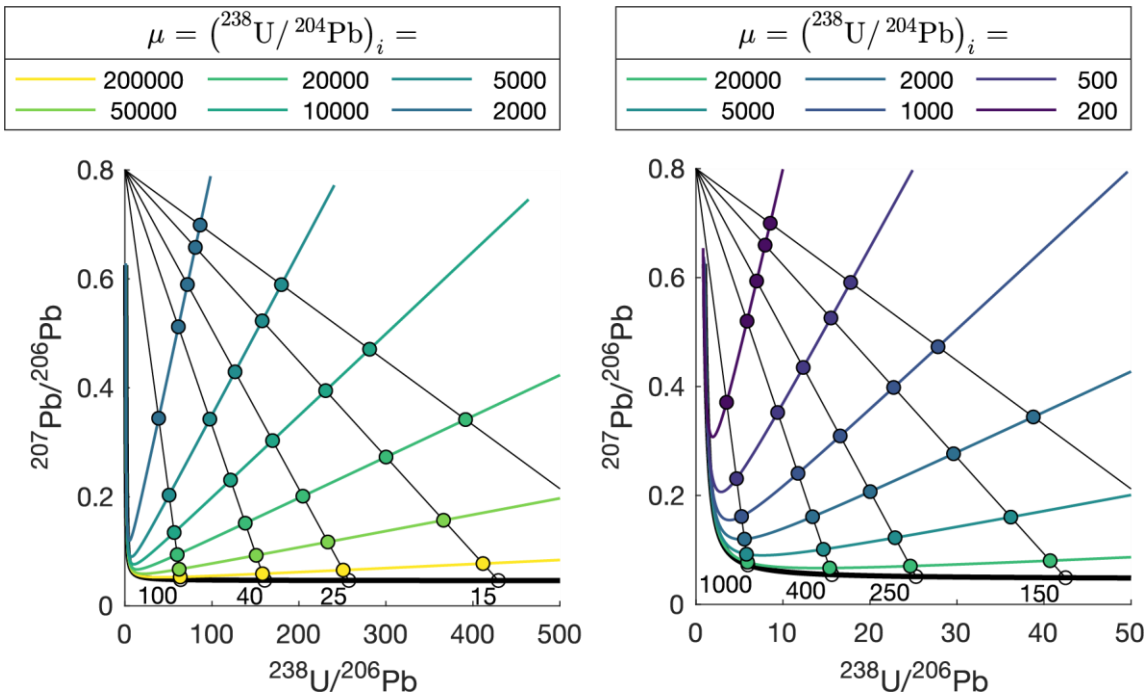

Figure 4. Tera-Wasserburg concordia plots of natural carbonate samples from a variety of settings, with no data rejection. Lower intercept dates are quoted without propagation of systematic uncertainties. See text for explanation.

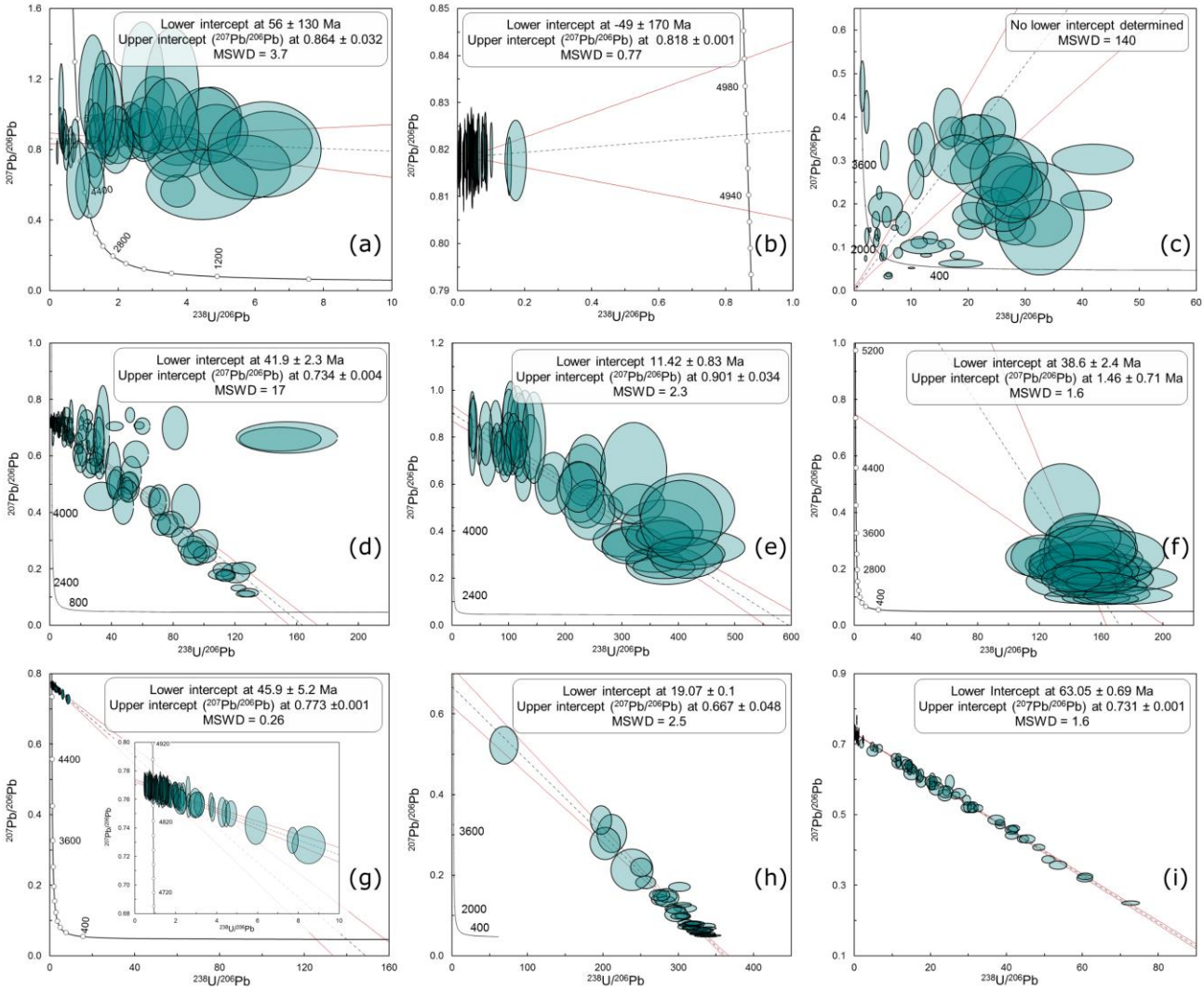

Figure 5. Uranium and total lead contents of various carbonate materials, plotted as 2D Kernel Density Estimates, based on a compilation of laser ablation spot data from the British Geological Survey lab over several years. Median values for high and low common-lead bearing U-Pb geochronometers, apatite and zircon, are shown for comparison.

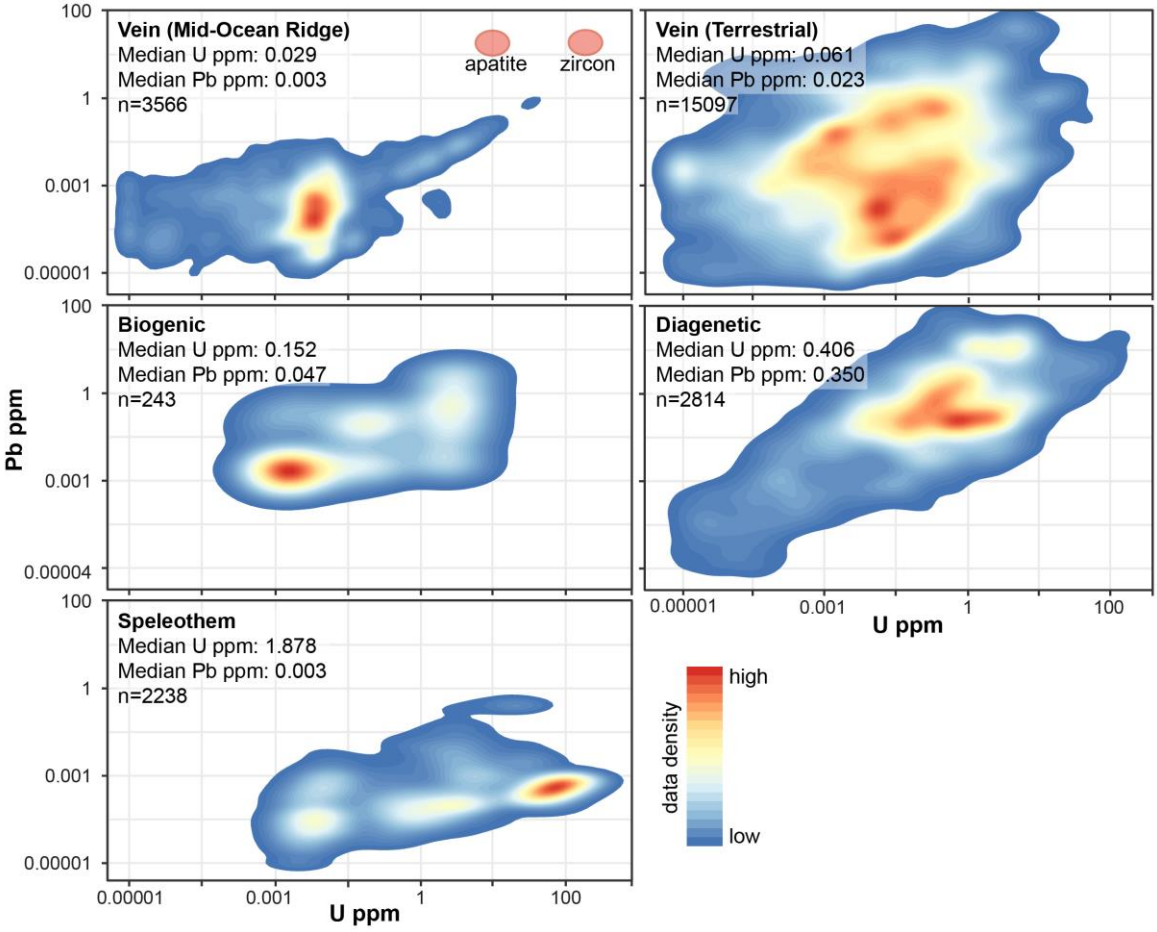

Figure 6. Example imagery from the range of techniques used for sample screening and characterisation. (a) mudstone-hosted vein calcite; (b) mudstone-hosted vein calcite; (c) carbonate concretion-hosted calcite vein; (d) individual calcite crystals grown in a fracture within crystalline bedrock; (e) calcite vein and cement within sediment-fill of an open fracture; (f) cave speleothem.

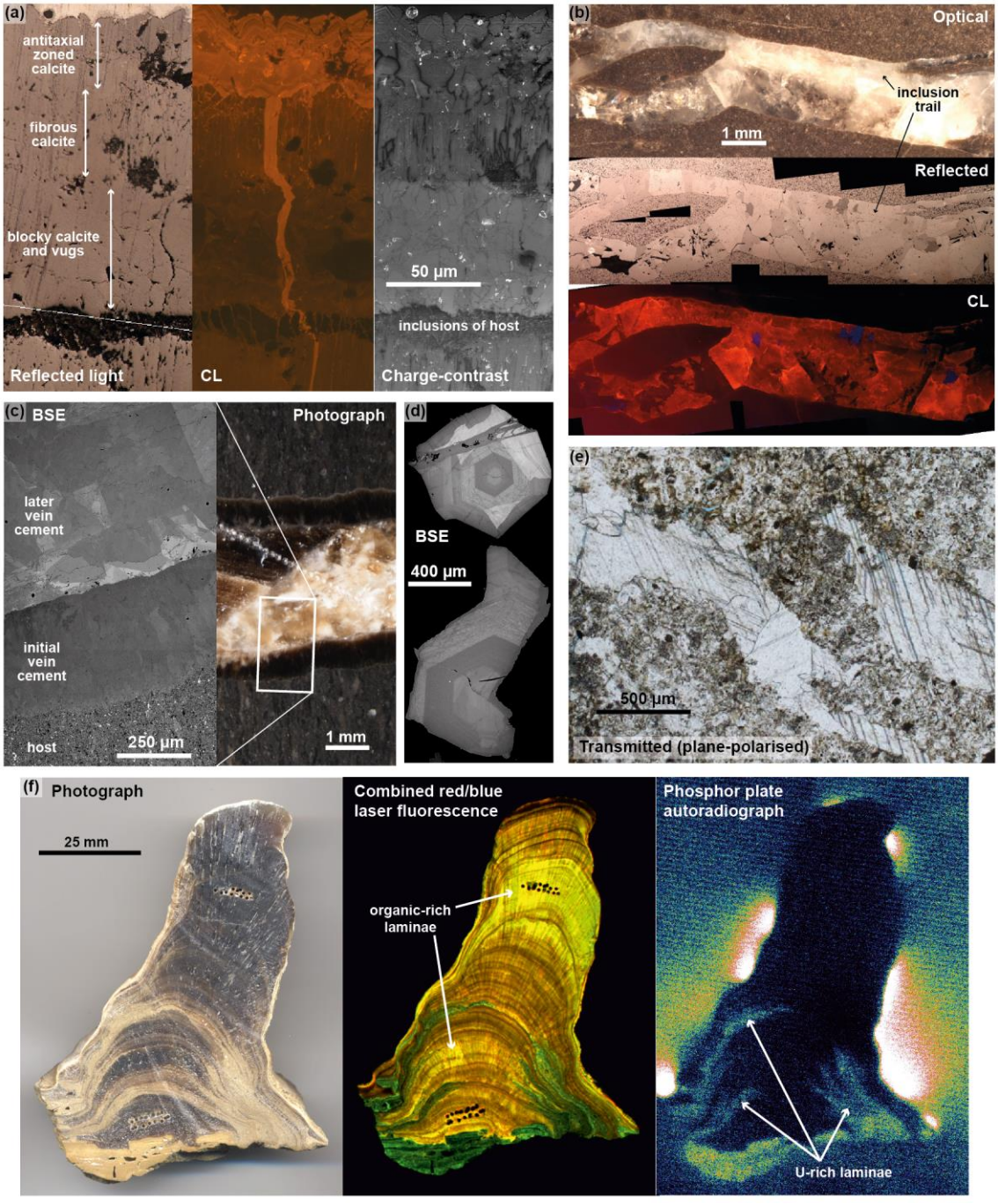

Figure 7. Photographs, LA-ICP-MS elemental maps, CL and CCI imagery and corresponding Tera-Wasserburg plots for four fracture-fill samples. For all maps, brighter =

1277 higher concentration. (a) Basalt-hosted fracture-fill calcite grown after zeolite, Faroe
1278 Islands. Three spot traverses for U-Pb data are shown, labelled i, ii and iii. (b) Basalt-hosted
1279 fracture-fill calcite, with zeolite grown after calcite, Faroe Islands. (c) Mudstone-hosted
1280 fracture-fill calcite, UK. U-Pb data are compared between a specific region avoiding the
1281 alteration, and from spot traverses across the sample. (d) Sandstone-hosted fracture-fill
1282 calcite, UK. CCI image is false-coloured. U-Pb data are shown with and without a rejection
1283 criteria based on removal of high Pb counts – corresponding to Pb-rich alteration pathways.

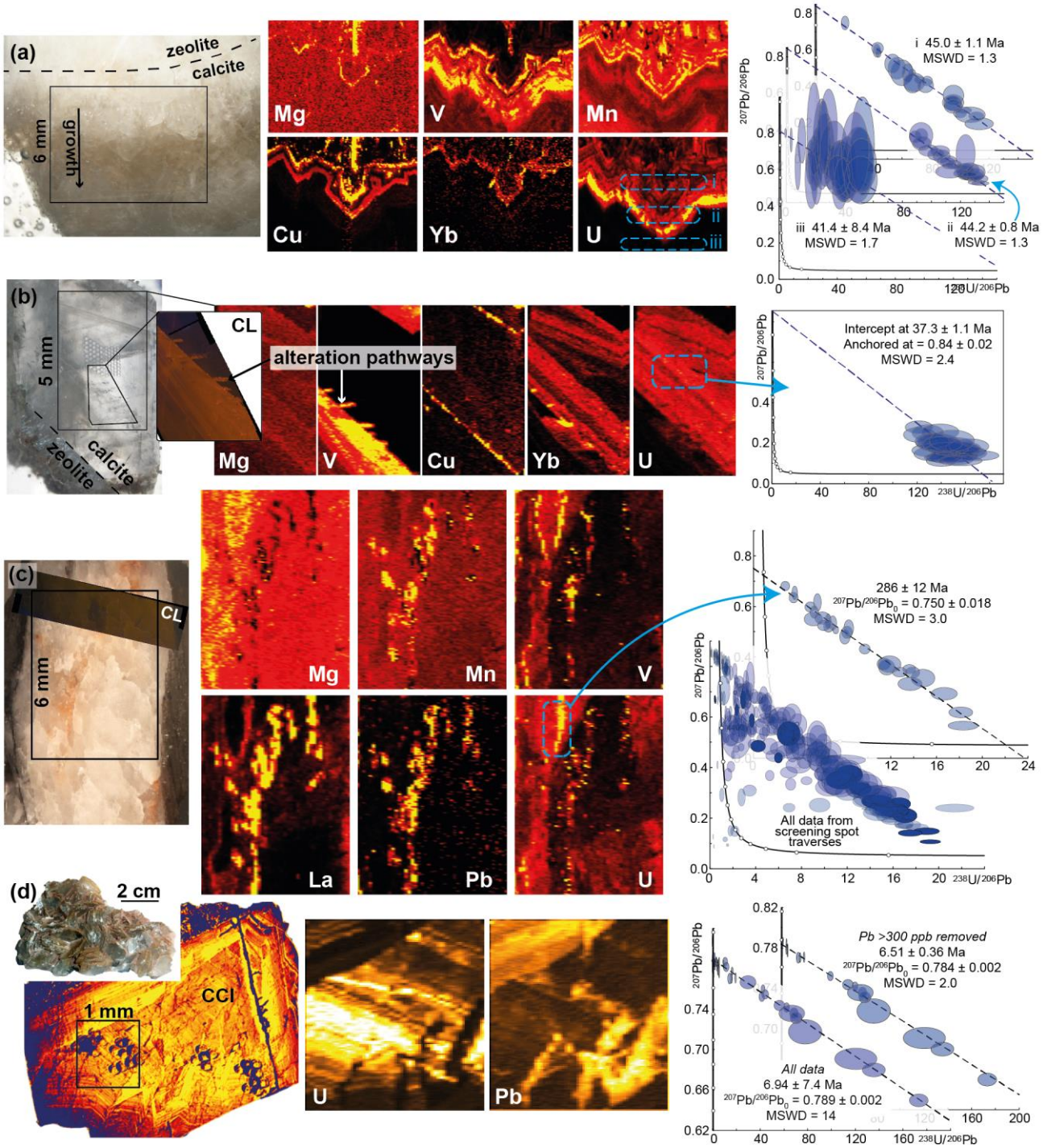

1284

Figure 8. Image-based dating (Monocle plug-in for Iolite) of sample BM18. (a) Trace element maps of the analysed region; (b) Photomicrograph of sample surface showing mapped region as U map; (c) U map showing the region of interest selected for the U-Pb date in green; (d) Tera-Wasserburg concordia of U-Pb data after pooling and filtering using the Monocle plug-in (see text for description).

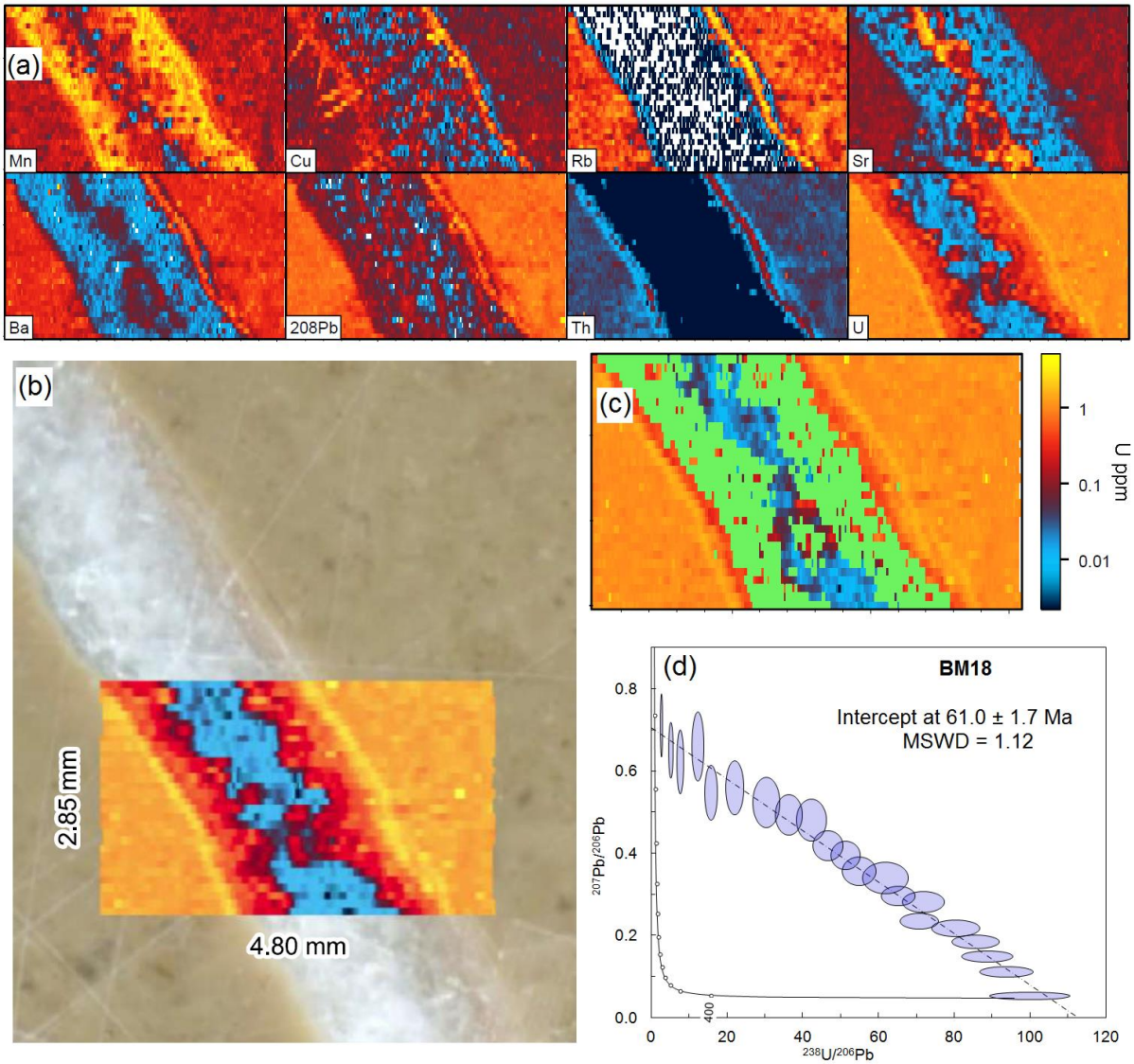

Figure 9. Image-based dating (Monocle plug-in for Iolite) of sample NR1511. (a) Trace element maps of the analysed region; (b) Photomicrograph of sample surface showing mapped region as U map; (c) U map showing the region of interest selected for the U-Pb date in green; (d) Tera-Wasserburg concordia of U-Pb data after pooling and filtering using the Monocle plug-in (see text for description).

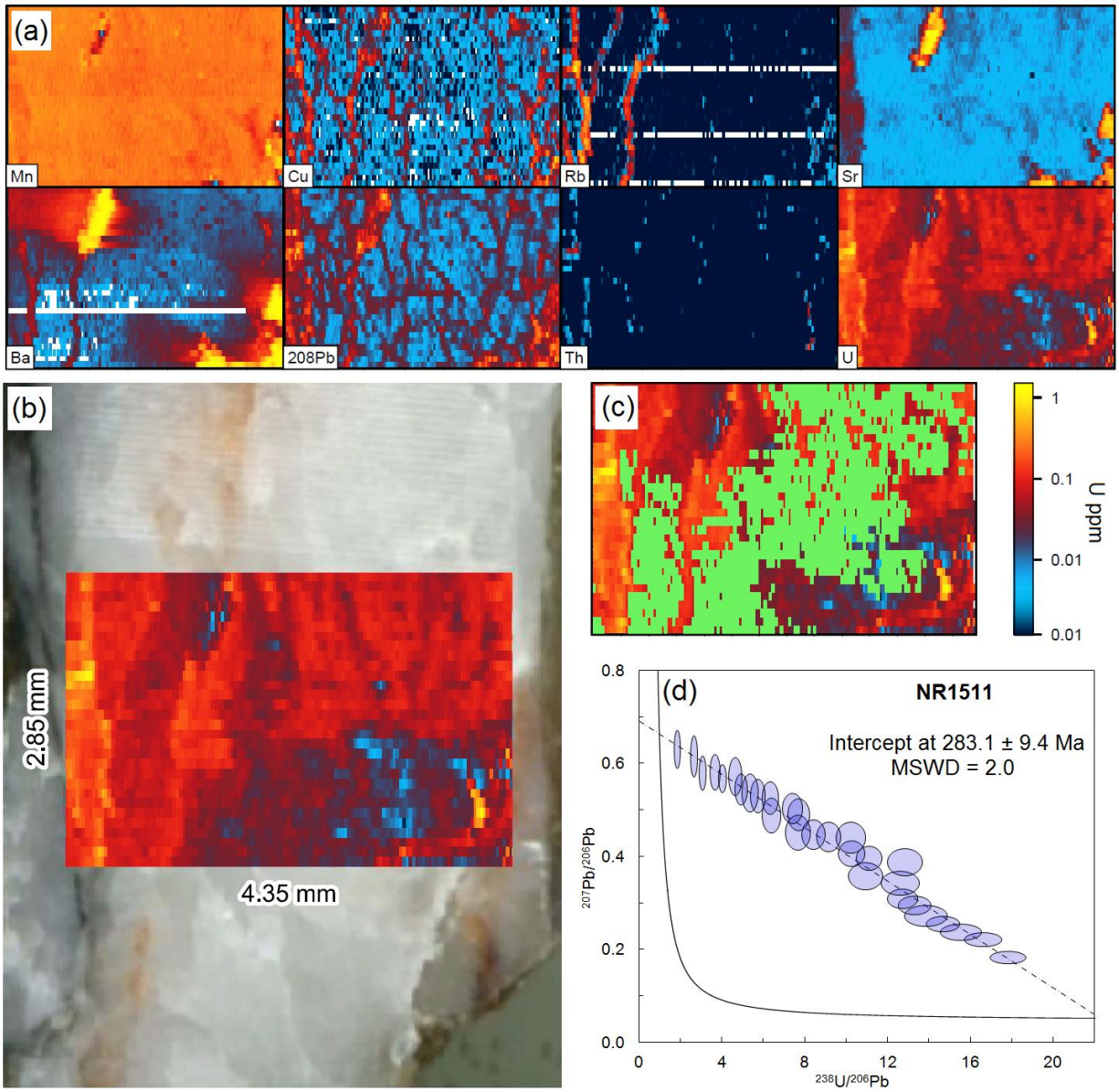

Figure 10. Compilation of upper intercept $^{207}Pb/^{206}Pb$ compositions from fracture-fill and diagenetic carbonates, of samples dated in the British Geological Survey laboratory (n=123). The grey curve is a Kernel Density Estimate showing the distribution of mean compositions. The red bar shows the Stacey and Kramers (1975) composition of terrestrial lead at present-day. Samples with very large uncertainties in the $^{207}Pb/^{206}Pb$ composition are those with very low Pb count-rates.

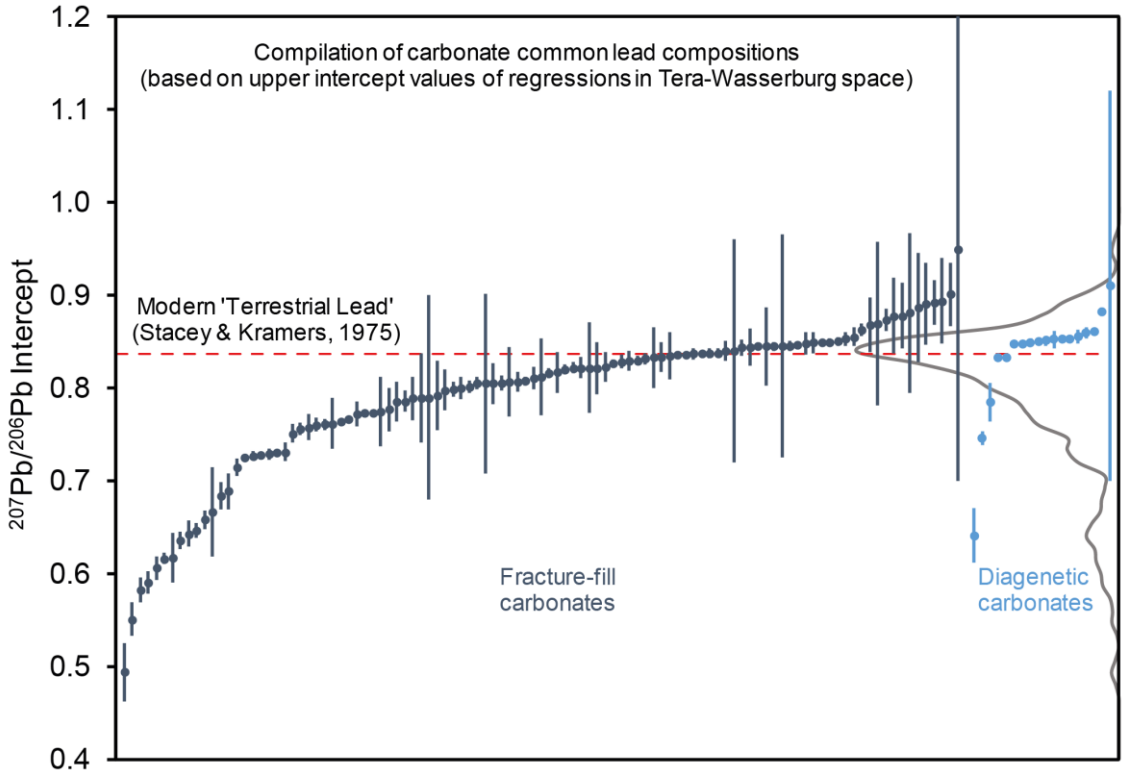

Figure 11. U-Pb data from a series of calcite veins (sample KH18) along the Moab Fault at Courthouse Junction, Utah. (a) Reflected light image of a region of veining showing the 100 µm spots; (b) Photomicrograph of the dated sample, with different dated domains of veining shown by blue, red, black and grey lines; (c) Tera-Wasserburg plot with U-Pb spot data colour-coded to match the different domains. The bars on the left show the variable $^{207}Pb/^{206}Pb$ upper intercept values for each domain.

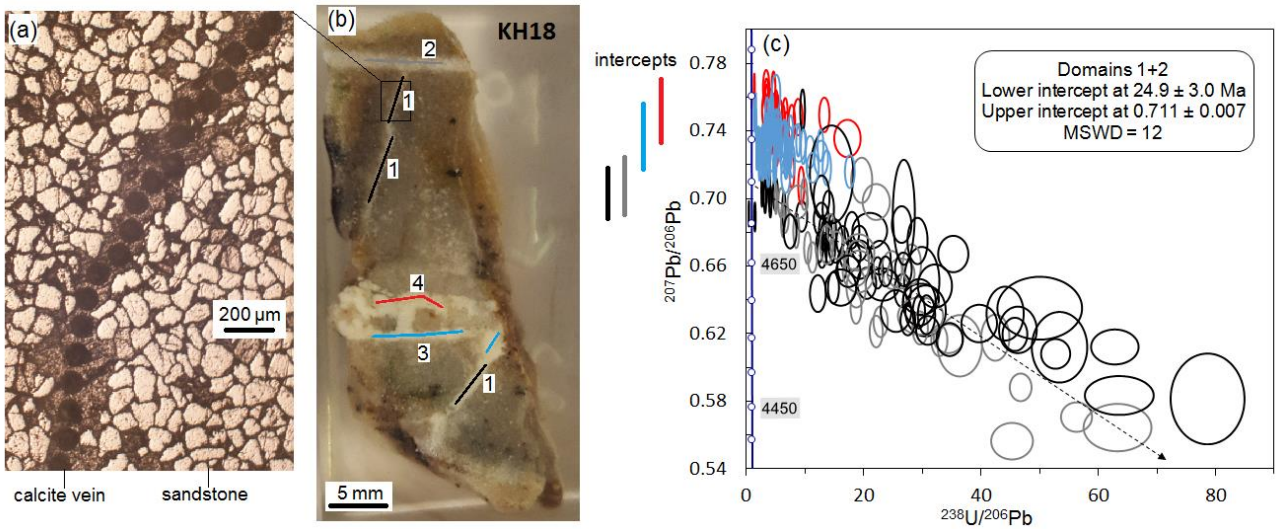

Figure 12. Compilation of uranium $^{234}U/^{238}U$ activity ratios from the literature of: (a) groundwater and deep brines - these are present-day $^{234}U/^{238}U$ values (note the compilation is dominated by shallow groundwater rather than brines); and (b) travertines and calcite precipitated in veins, commonly but not exclusively associated with travertines – these are estimated $^{234}U/^{238}U_0$ values.

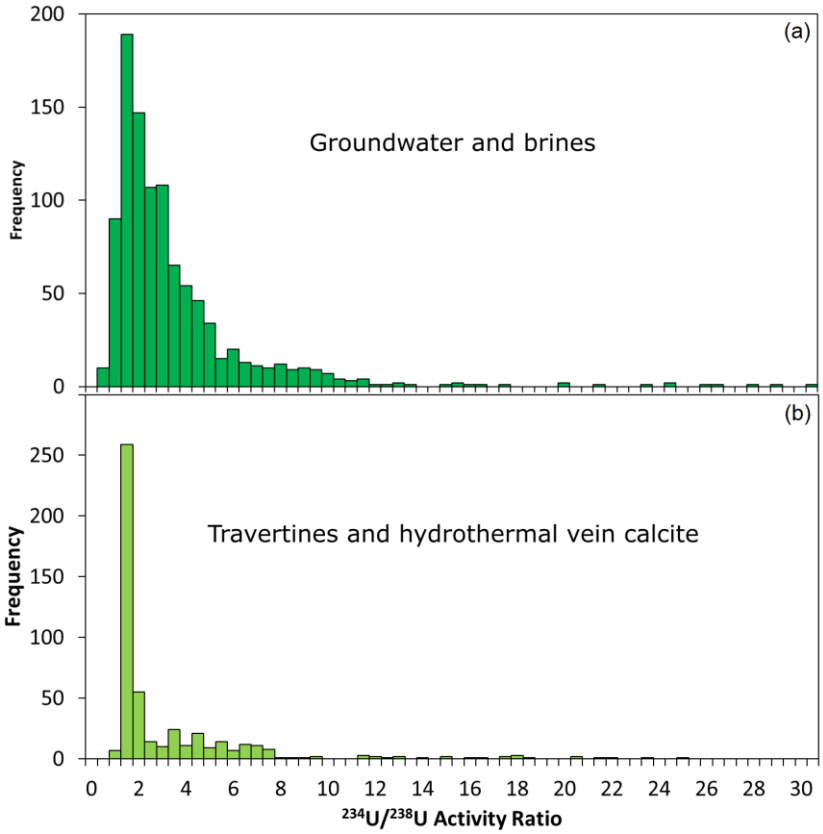

Figure 13. Curves in different colours showing how an individual $^{206}Pb/^{238}U$ age (y-axis) will vary with a change in the initial $^{234}U/^{238}U$ activity ratio (x-axis). For example, a sample providing a measured $^{206}Pb/^{238}U$ age of 5 Ma will actually have a true age of 3.1 Ma if the initial $^{234}U/^{238}U$ is as high as 6. The grey histogram shows the combined compilations of groundwater, travertine and vein data from Figure 12.

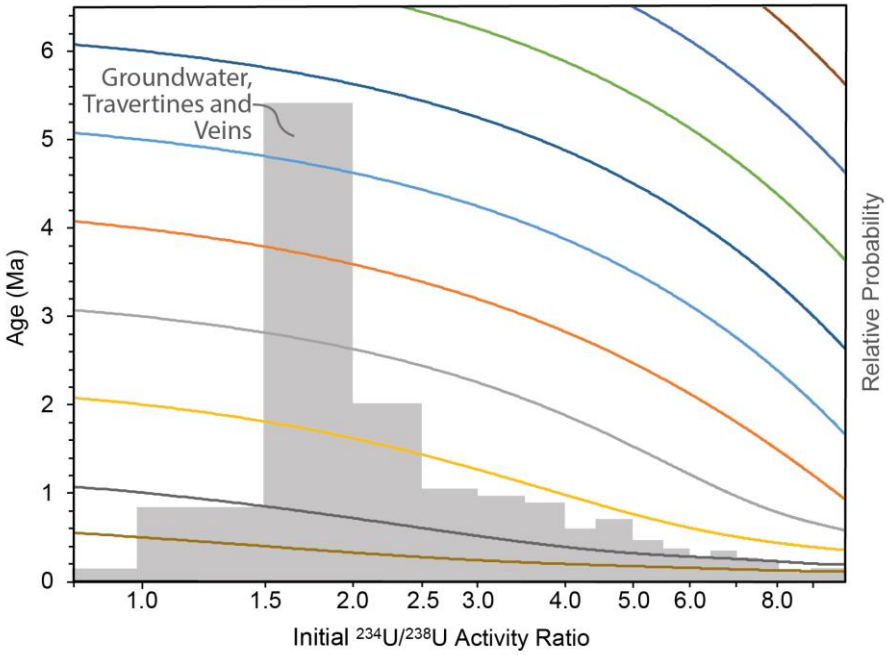

Figure 14. Tera-Wasserburg plots for LA-ICP-MS U-Pb data from two slicken-fibre calcite samples that exhibit potential open system behaviour caused by U mobility. Vectors for U loss and gain are schematic. Evidence for such U mobilisation requires additional lines of evidence that are currently lacking.

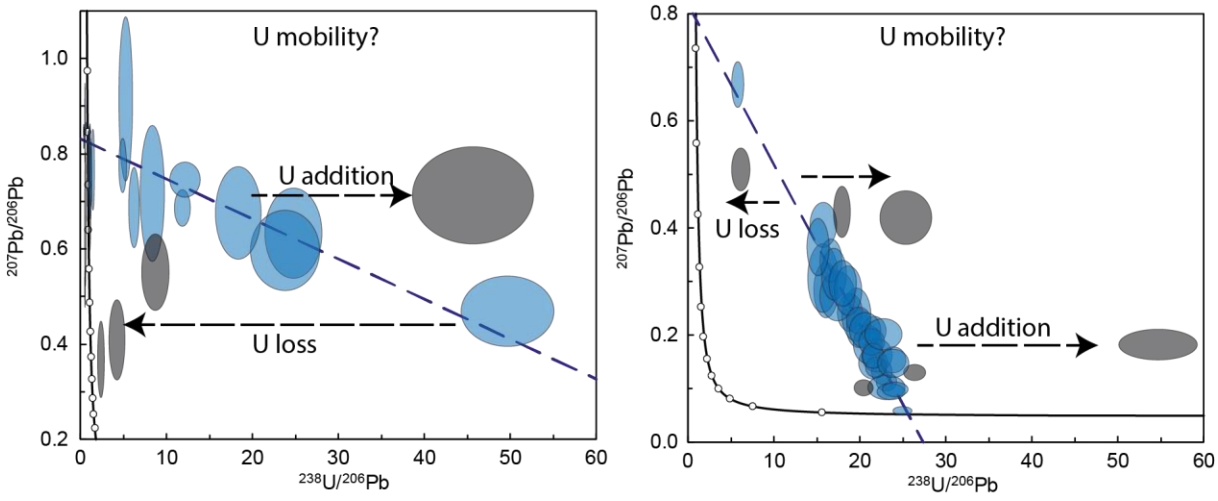

Figure 15. Compilation of published LA-ICP-MS U-Pb dates of carbonate (n=318). A) MSWD plotted against $^{206}Pb/^{238}U$ age; and B) Precision as 2s % plotted against $^{206}Pb/^{238}U$ age. The histograms in the background show the distribution of dates.

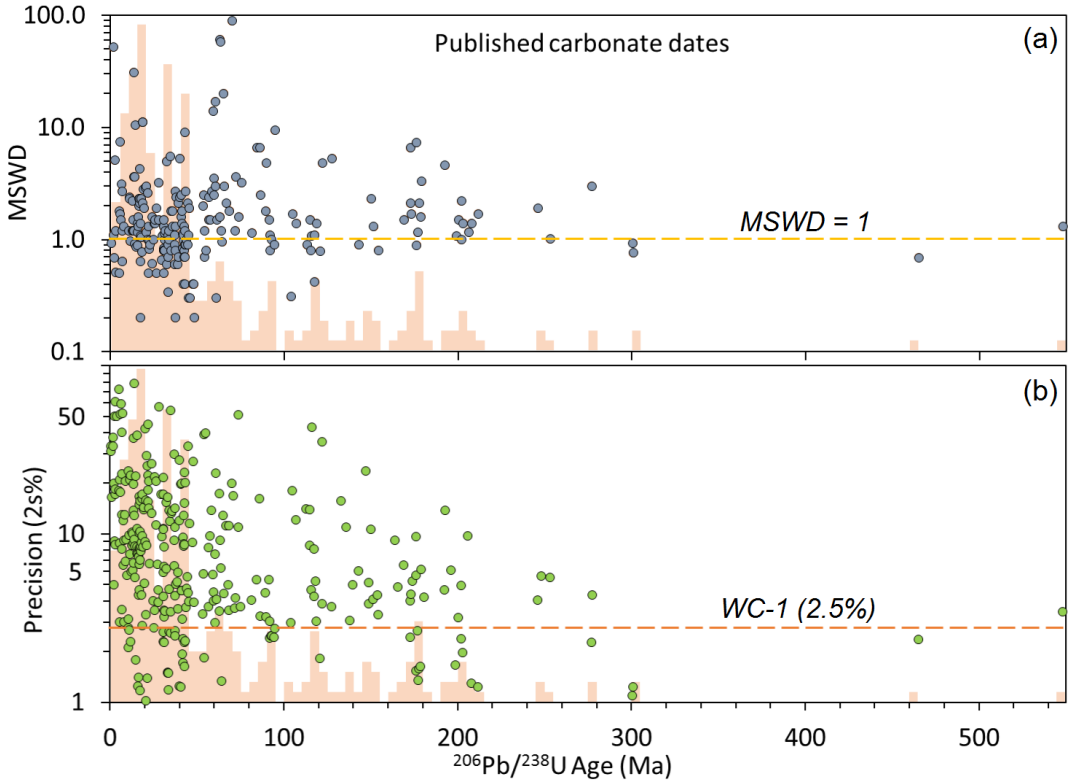

16. Appendix A

16.1. Implications of age data

The focus of this paper is not on the meaning of the age data presented, or its implications for faulting or fluid-flow; however, we provide brief information for interested readers.

16.1. Figure 7a and 7b - Faroe Island brittle faults

The significance of the Eocene ages has been discussed by Roberts & Walker (2016). This paper was the first to demonstrate the applicability of LA-ICP-MS U-Pb carbonate geochronology to dating brittle structures in the upper crust.

16.2. Figure 7c and 9 - Variscan-related vein in the Northumberland Basin

The age of ca. 287 Ma for the dated calcite crystal can be linked to deformation of the host rock based on the vein structure. The calcite is taken from a planar fracture forming on the axial plane of a small fold that has accommodated bedding-plane sliding (Fig. 8). The fracture is filled with calcite mineralisation of the stretched vein type (Bons et al., 2012), and that is interpreted to have formed soon after opening of the vein, and synchronous with deformation. The age of ca. 287 Ma broadly overlaps with the intrusion of the Whin Sill (ca. 297 Ma; Heaman pers. comm. within De Paola et al., 2005), and is therefore compatible with the model of partitioned transpression of De Paola et al. (2005), who suggest that deformation was synchronous with the Whin Sill intrusion.

16.3. Figure 7d - Sellafield fracture mineralisation

Sample 877 was collected from the modern-day saline transition zone between the upper fresh groundwater system and the deeper saline basinal-basement groundwater system, at a depth of -635 m OD within the St Bees Sandstone Group (Triassic) in Sellafield borehole BH10A (equivalent to sample B697 and D750: Appendix Table S2, Milodowski et al., 2018). Externally, this calcite exhibits a “nailhead” (i.e. c-axis flattened) crystal habit (Figure 10). However, detailed petrographic analysis reveals it has a complex growth history: comprising of cores of c-axis-elongated calcite characteristic of the deeper saline groundwater that are syntaxially-overgrown by later equant and c-axis flattened calcite characteristic of the overlying fresh groundwater zone (Milodowski et al., 2018). The U-Pb

analyses all come from within the saline groundwater zone type calcite core region (rather than the later freshwater-type overgrowth that has extremely low U).

Late-stage (generation “ME9”) calcite is a characteristic feature of the present-day fracture-controlled deep groundwater system in the Sellafield area of the west Cumbrian coastal plain (Milodowski et al., 2018). The resulting age suggests that ME9 calcite growth in the sampled fracture was initiated in the late Miocene, and has been preserved (or at least partially preserved until the present-day). The implication is that the modern groundwater system was developed following regional Miocene uplift and younger groundwater recharge relating to glaciations and/or uplift of the region, have not led to complete re-precipitation of fracture-filling calcite, with calcite precipitation continuing to the present-day. Taken together with other petrographic, stable isotope, strontium isotope, fluid inclusion, microchemical analyses and whole-crystal U-Th age dating, the age data support the interpretation that despite evidence for glacial recharge, the geochemical conditions (e.g. pH, Eh) have remained stable over this period at potential repository depths (cf. Milodowski et al., 2018).

16.4. Figure 8 – Vein set of the Bighorn Basin, Wyoming

This sample is from a vein set in the sedimentary cover of the Bighorn Basin, and is part of a larger study that analysed the timing of deformation in the foreland of the Sevier and Laramide orogenies, and how this deformation propagated in time and space (Beaudoin et al., 2018).

16.5. Figure 11 - Moab fault

This sample comprises multiple thin (1 to 5 mm wide) veins collected from the footwall damage zone of the Moab Fault in southeast Utah. Regional deformation is primarily driven by salt tectonics (Gutierrez, 2004), and salt dissolution has produced up to one km of offset within the sedimentary rocks along the Moab Fault (Foxford et al., 1996). Fault zone deformation was closely associated with fluid flow and carbonate cementation (Eichhubl et al., 2009; Hodson et al., 2016). Ar-Ar ages from clay fault gauge range from 63 to 43 Ma and are interpreted to record the final episodes of faulting and fracture generation (Pevear et al., 1997; Solum et al., 2005). Our new lower intercept age of 22 Ma is imprecise, but

clearly younger than the early-Tertiary ages. This suggests that circulating fluids continued to move along the fault zone long after the cessation of fault related deformation.

17. References

1. Albut, G., Kamber, B.S., Brüske, A., Beukes, N.J., Smith, A.J. and Schoenberg, R.: Modern weathering in outcrop samples versus ancient paleoredox information in drill core samples from a Mesoarchaean marine oxygen oasis in Pongola Supergroup, South Africa. *Geochimica et Cosmochimica Acta*, *265*, 330-353, 2019.
2. Babinski, M., Van Schmus, W.R. and Chemale Jr, F.: Pb–Pb dating and Pb isotope geochemistry of Neoproterozoic carbonate rocks from the São Francisco basin, Brazil: implications for the mobility of Pb isotopes during tectonism and metamorphism. *Chemical Geology*, *160*, 175-199, 1999.
3. Babinski, M., Vieira, L.C. and Trindade, R.I.: Direct dating of the Sete Lagoas cap carbonate (Bambuí Group, Brazil) and implications for the Neoproterozoic glacial events. *Terra Nova*, *19*, 401-406, 2007.
4. Baker, A., Smart, P.L., Barnes, W.L., Edwards, R.L. and Farrant, A.: The Hekla 3 volcanic eruption recorded in a Scottish speleothem?. *The Holocene*, *5*, 336-342, 1995.
5. Baker, A., Smith, C.L., Jex, C., Fairchild, I.J., Genty, D. and Fuller, L.: Annually laminated speleothems: a review. *International Journal of Speleology*, *37*, 193-206, 2008.
6. Barnaby, R.J. and Rimstidt, J.D.: Redox conditions of calcite cementation interpreted from Mn and Fe contents of authigenic calcites. *GSA Bulletin*, *101*, 795-804, 1989.
7. Beaudoin, N., Lacombe, O., Roberts, N.M. and Koehn, D.: U-Pb dating of calcite veins reveals complex stress evolution and thrust sequence in the Bighorn Basin, Wyoming, USA. Geology, 46, 1015-1018, 2018.
8. Bertok, C., Barale, L., d'Atri, A., Martire, L., Piana, F., Rossetti, P. and Gerdes, A., 2019. Unusual marbles in a non-metamorphic succession of the SW Alps (Valdieri, Italy) due to early Oligocene hydrothermal flow. International Journal of Earth Sciences, 1-20, 2019.
9. Bons, P.D., Elburg, M.A. and Gomez-Rivas, E.: A review of the formation of tectonic veins and their microstructures. *Journal of Structural Geology*, *43*, 33-62, 2012.

10. Brannon, J.C., Cole, S.C., Podosek, F.A., Ragan, V.M., Coveney, R.M., Wallace, M.W. and Bradley, A.J.: Th-Pb and U-Pb dating of ore-stage calcite and Paleozoic fluid flow. *Science*, *271*, 491-493, 1996.
11. Buckman, J.O., Corbett, P.W. and Mitchell, L.: Charge contrast imaging (CCI): revealing enhanced diagenetic features of a coquina limestone. *Journal of Sedimentary Research*, *86*, 734-748, 2016.
12. Burisch, M., Gerdes, A., Walter, B.F., Neumann, U., Fettel, M. and Markl, G.: Methane and the origin of five-element veins: mineralogy, age, fluid inclusion chemistry and ore forming processes in the Odenwald, SW Germany. Ore Geology Reviews, 81, 42-61, 2017.
13. Burisch, M., Walter, B.F., Gerdes, A., Lanz, M. and Markl, G.: Late-stage anhydrite-gypsum-siderite-dolomite-calcite assemblages record the transition from a deep to a shallow hydrothermal system in the Schwarzwald mining district, SW Germany. Geochimica et Cosmochimica Acta, 223, 259-278, 2018.
14. Burn, M., Lanari, P., Pettke, T. and Engi, M.: Non-matrix-matched standardisation in LA-ICP-MS analysis: general approach, and application to allanite Th–U–Pb dating. *Journal of analytical atomic spectrometry*, *32*, 1359-1377, 2017.
15. Cherniak, D.J.: An experimental study of strontium and lead diffusion in calcite, and implications for carbonate diagenesis and metamorphism. *Geochimica et Cosmochimica Acta*, *61*, 4173-4179, 1997.
16. Cole, J.M., Nienstedt, J., Spataro, G., Rasbury, E.T., Lanzirotti, A., Celestian, A.J., Nilsson, M. and Hanson, G.N.: Phosphor imaging as a tool for in situ mapping of ppm levels of uranium and thorium in rocks and minerals. *Chemical Geology*, *193*, 127-136, 2003.
17. Cole, J.M., Rasbury, E.T., Hanson, G.N., Montañez, I.P. and Pedone, V.A.: Using U-Pb ages of Miocene tufa for correlation in a terrestrial succession, Barstow Formation, California. *Geological Society of America Bulletin*, *117*, 276-287, 2005.
18. Coogan, L.A., Parrish, R.R. and Roberts, N.M.: Early hydrothermal carbon uptake by the upper oceanic crust: Insight from in situ U-Pb dating. Geology, 44, 147-150, 2016.
19. Cuthbert, S.J. and Buckman, J.O.: Charge contrast imaging of fine-scale microstructure and compositional variation in garnet using the environmental scanning electron microscope. *American Mineralogist*, *90*, 701-707, 2005.

20. De Paola, N., Holdsworth, R.E., McCaffrey, K.J. and Barchi, M.R.: Partitioned transtension: an alternative to basin inversion models. *Journal of Structural Geology*, *27*, 607-625, 2005.
21. DeWolf, C.P. and Halliday, A.N.: U-Pb dating of a remagnetized Paleozoic limestone. *Geophysical Research Letters*, *18*, 1445-1448, 1991.
22. Drake, H., Heim, C., Hogmalm, K.J. and Hansen, B.T.: Fracture zone-scale variation of trace elements and stable isotopes in calcite in a crystalline rock setting. *Applied Geochemistry*, *40*, 11-24, 2014.
23. Drake, H., Heim, C., Roberts, N.M.W., Zack, T., Tillberg, M., Broman, C., Ivarsson, M., Whitehouse, M.J. and Åström, M.E.: Isotopic evidence for microbial production and consumption of methane in the upper continental crust throughout the Phanerozoic eon. Earth and Planetary Science Letters, 470, 108-118, 2017.
24. Drake, H., Mathurin, F.A., Zack, T., Schäfer, T., Roberts, N.M.W., Whitehouse, M., Karlsson, A., Broman, C. and Åström, M.E.: Incorporation of metals into calcite in a deep anoxic granite aquifer. *Environmental science & technology*, *52*, 493-502, 2018.
25. Drake, H., Roberts, N.M.W., Heim, C., Whitehouse, M.J., Siljeström, S., Kooijman, E., Broman, C., Ivarsson, M. and Åström, M.E., 2019. Timing and origin of natural gas accumulation in the Siljan impact structure, Sweden. *Nature communications*, *10*, 1-14.
26. Drake, H., Tullborg, E.L., Hogmalm, K.J. and Åström, M.E.: Trace metal distribution and isotope variations in low-temperature calcite and groundwater in granitoid fractures down to 1 km depth. *Geochimica et Cosmochimica Acta*, *84*, 217-238, 2012.
27. Drost, K., Chew, D., Petrus, J.A., Scholze, F., Woodhead, J.D., Schneider, J.W. and Harper, D.A.: An Image Mapping Approach to U-Pb LA-ICP-MS Carbonate Dating, and Applications to Direct Dating of Carbonate Sedimentation. Geochemistry, Geophysics, Geosystems, 19, 4631-4648, DOI:10.1029/2018GC007850, 2018.
28. Eichhubl, P., Davatz, N.C. and Becker, S.P.: Structural and diagenetic control of fluid migration and cementation along the Moab fault, Utah. *AAPG bulletin*, *93*, 653-681, 2009.
29. Eiler, J.M.: “Clumped-isotope” geochemistry—The study of naturally-occurring, multiply-substituted isotopologues. *Earth and planetary science letters*, *262*, 309-327, 2007.

30. Engel, J., Woodhead, J., Hellstrom, J., Maas, R., Drysdale, R. and Ford, D.: Corrections for initial isotopic disequilibrium in the speleothem U-Pb dating method. *Quaternary Geochronology*, *54*, 101009, 2019.
31. Engi, M., Lanari, P. and Kohn, M.J.: Significant ages—An introduction to petrochronology. *Reviews in Mineralogy and Geochemistry*, *83*, 1-12, 2017.
32. Fairey, B., Tsikos, H., Corfu, F. and Polteau, S.: U–Pb systematics in carbonates of the Postmasburg Group, Transvaal Supergroup, South Africa: primary versus metasomatic controls. *Precambrian Research*, *231*, 194-205, 2013.
33. Field, L.P., Milodowski, A.E., Evans, D., Palumbo-Roe, B., Hall, M.R., Marriott, A.L., Barlow, T. and Devez, A.: Determining constraints imposed by salt fabrics on the morphology of solution-mined energy storage cavities, through dissolution experiments using brine and seawater in halite. *Quarterly Journal of Engineering Geology and Hydrogeology*, *52*, 240-254, 2019.
34. Flude, S., Lee, M.R., Sherlock, S.C. and Kelley, S.P.: Cryptic microtextures and geological histories of K-rich alkali feldspars revealed by charge contrast imaging. *Contributions to Mineralogy and Petrology*, *163*, 983-994, 2012.
35. Foxford, K.A., Garden, I.R., Guscott, S.C., Burley, S.D., Lewis, J.J.M., Walsh, J.J. and Watterson, J.: The field geology of the Moab fault, in: Geology and Resources of the Paradox Basin, Utah Geological Association, 25, 265-283, 1996.
36. Godeau, N., Deschamps, P., Guihou, A., Leonide, P., Tendil, A., Gerdes, A., Hamelin, B. and Girard, J.P.: U-Pb dating of calcite cement and diagenetic history in microporous carbonate reservoirs: Case of the Urgonian Limestone, France. Geology, 46, 247-250, 2018.
37. Goodfellow, B.W., Viola, G., Bingen, B., Nuriel, P. and Kylander-Clark, A.R.: Palaeocene faulting in SE Sweden from U–Pb dating of slickenfibre calcite. Terra Nova, 29, 321-328, 2017.
38. Grandia, F., Asmerom, Y., Getty, S., Cardellach, E. and Canals, A.: U–Pb dating of MVT ore-stage calcite: implications for fluid flow in a Mesozoic extensional basin from Iberian Peninsula. *Journal of Geochemical Exploration*, *69*, 377-380, 2000.
39. Hansman, R.J., Albert, R., Gerdes, A. and Ring, U.: Absolute ages of multiple generations of brittle structures by U-Pb dating of calcite. Geology, 46, 207-210, 2018.

40. Hareyama, M., Tsuchiya, N., Takebe, M. and Chida, T.: Two dimensional measurement of natural radioactivity of granitic rocks by photostimulated luminescence technique. *Geochemical Journal*, *34*, 1-9, 2000.
41. Hellwig, A., Voigt, S., Mulch, A., Frisch, K., Bartenstein, A., Pross, J., Gerdes, A. and Voigt, T.: Late Oligocene to early Miocene humidity change recorded in terrestrial sequences in the Ili Basin (south-eastern Kazakhstan, Central Asia). Sedimentology, 65, 517-539, 2018.
42. Hodson, K.R., Crider, J.G. and Huntington, K.W.: Temperature and composition of carbonate cements record early structural control on cementation in a nascent deformation band fault zone: Moab Fault, Utah, USA. *Tectonophysics*, *690*, 240-252, 2016.
43. Holdsworth, R.E., McCaffrey, K.J.W., Dempsey, E., Roberts, N.M.W., Hardman, K., Morton, A., Feely, M., Hunt, J., Conway, A. and Robertson, A.: Natural fracture propping and earthquake-induced oil migration in fractured basement reservoirs. Geology, in press, DOI:10.1130/G46280.1, 2019.
44. Hopley, P.J., Reade, H., Parrish, R., De Kock, M. and Adams, J.W.: Speleothem evidence for C3 dominated vegetation during the Late Miocene (Messinian) of South Africa. *Review of Palaeobotany and Palynology*, *264*, 75-89, 2019.
45. Horstwood, M.S.A., Košler, J., Gehrels, G., Jackson, S.E., McLean, N.M., Paton, C., Pearson, N.J., Sircombe, K., Sylvester, P., Vermeesch, P. and Bowring, J.F.: Community-derived standards for LA-ICP-MS U-(Th-) Pb geochronology–Uncertainty propagation, age interpretation and data reporting. *Geostandards and Geoanalytical Research*, *40*, 311-332, 2016.
46. Incerpi, N., Martire, L., Manatschal, G., Bernasconi, S.M., Gerdes, A., Czuppon, G., Palcsu, L., Karner, G.D., Johnson, C.A. and Figueredo, P.H.: Hydrothermal fluid flow associated to the extensional evolution of the Adriatic rifted margin: Insights from the pre-to post-rift sedimentary sequence (SE Switzerland, N ITALY). Basin Research, in press, DOI:10.1111/bre.12370, 2019.
47. Jahn, B.M.: Pb–Pb dating of young marbles from Taiwan. *Nature*, *332*, 429, 1988.
48. Jahn, B.M. and Cuvellier, H.: Pb-Pb and U-Pb geochronology of carbonate rocks: an assessment. *Chemical Geology*, *115*, 125-151, 1994.

49. Johansson, Å. and Rickard, D., 1984. Isotopic composition of Phanerozoic ore leads from the Swedish segment of the Fennoscandian Shield. *Mineralium Deposita*, *19*(4), pp.249-255.
50. Jones, C.E., Halliday, A.N. and Lohmann, K.C.: The impact of diagenesis on high-precision U-Pb dating of ancient carbonates: An example from the Late Permian of New Mexico. *Earth and Planetary Science Letters*, *134*, 409-423, 1995.
51. Kelly, S.D., Newville, M.G., Cheng, L., Kemner, K.M., Sutton, S.R., Fenter, P., Sturchio, N.C. and Spötl, C.: Uranyl incorporation in natural calcite. *Environmental Science & Technology*, *37*, 1284-1287, 2003.
52. Kreissl, S., Gerdes, A., Walter, B.F., Neumann, U., Wenzel, T., Markl, G.: Reconstruction of a >200 Ma multi-stage “five element” Bi-Co-Ni-Fe-As-S system in the Penninic Alps, Switzerland. Ore Geology Reviews 95, 746-788, 2018.
53. Kronfeld, J., Vogel, J.C. and Talma, A.S.: A new explanation for extreme $^{234}U/^{238}U$ disequilibria in a dolomitic aquifer. *Earth and Planetary Science Letters*, *123*, 81-93, 1994.
54. Kylander-Clark, A.R., Hacker, B.R. and Cottle, J.M.: Laser-ablation split-stream ICP petrochronology. *Chemical Geology*, *345*, 99-112, 2013.
55. Langmuir, D.: Uranium solution-mineral equilibria at low temperatures with applications to sedimentary ore deposits. *Geochimica et Cosmochimica Acta*, *42*, 547-569, 1978.
56. Lawson, M., Shenton, B.J., Stolper, D.A., Eiler, J.M., Rasbury, E.T., Becker, T.P., Phillips-Lander, C.M., Buono, A.S., Becker, S.P., Pottorf, R. and Gray, G.G.: Deciphering the diagenetic history of the El Abra Formation of eastern Mexico using reordered clumped isotope temperatures and U-Pb dating. GSA Bulletin, 130, 617-629, 2018.
57. Lee, M.R., Hodson, M.E. and Langworthy, G.: Earthworms produce granules of intricately zoned calcite. *Geology*, *36*, 943-946, 2008.
58. Li, Q., Parrish, R.R., Horstwood, M.S.A. and McArthur, J.M.: U–Pb dating of cements in Mesozoic ammonites. Chemical Geology, 376, 76-83, 2014.
59. Liivamägi S, Środon J, Bojanowski M, Gerdes A, Stanek JJ, Williams L, Szczerba M.: Paleosols on the Ediacaran basalts of the East European Craton: a unique record of paleoweathering with minimum diagenetic overprint. Precambrian Research, 316, 66-82, 2018.

60. MacDonald, J.M., Faithfull, J.W., Roberts, N.M.W., Davies, A.J., Holdsworth, C.M., Newton, M., Williamson, S., Boyce, A. and John, C.M.: Clumped-isotope palaeothermometry and LA-ICP-MS U–Pb dating of lava-pile hydrothermal calcite veins. *Contributions to Mineralogy and Petrology*, *174*, 63, 2019.
61. Machel, H.G.: Cathodoluminescence in calcite and dolomite and its chemical interpretation. *Geoscience Canada*, *12*, 139-147, 1985.
62. Machel, H.G.: Application of cathodoluminescence to carbonate diagenesis, in: *Cathodoluminescence in geosciences*, edited by Pagel M., Barbin V., Blanc P. and Ohnenstetter D., Springer, Berlin, Heidelberg, Germany, 271-301, 2000.
63. Mangenot, X., Gasparrini, M., Gerdes, A., Bonifacie, M. and Rouchon, V.: An emerging thermochronometer for carbonate-bearing rocks: ∆47/(U-Pb). Geology, 46, 1067-1070, 2018.
64. Maskenskaya, O.M., Drake, H., Broman, C., Hogmalm, J.K., Czuppon, G. and Åström, M.E.: Source and character of syntaxial hydrothermal calcite veins in Paleoproterozoic crystalline rocks revealed by fine-scale investigations. *Geofluids*, *14*, 495-511, 2014.
65. Mazurek, M., Davis, D.W., Madritsch, H., Rufer, D., Villa, I.M., Sutcliffe, C.N., De Haller, A. and Traber, D.: Veins in clay-rich aquitards as records of deformation and fluid-flow events in northern Switzerland. Applied Geochemistry, 95, 57-70, 2018.
66. Methner, K., Mulch, A., Fiebig, J., Wacker, U., Gerdes, A., Graham, S.A. and Chamberlain, C.P.: Rapid middle Eocene temperature change in western North America. Earth and Planetary Science Letters, 450, 132-139, 2016.
67. Michie, U.M. and Bowden, R.A.: UK NIREX geological investigations at Sellafield. *Proceedings of the Yorkshire Geological Society*, *50*, 5-9, 1994.
68. Milodowski, A.E., Bath, A. and Norris, S.: Palaeohydrogeology using geochemical, isotopic and mineralogical analyses: Salinity and redox evolution in a deep groundwater system through Quaternary glacial cycles. *Applied geochemistry*, *97*, 40-60, 2018.
69. Milton, G.M. and Brown, R.M.: Adsorption of uranium from groundwater by common fracture secondary minerals. *Canadian Journal of Earth Sciences*, *24*, 1321-1328, 1987.
70. Moorbath, S., Taylor, P.N., Orpen, J.L., Treloar, P. and Wilson, J.F.: First direct radiometric dating of Archaean stromatolitic limestone. *Nature*, *326*, 865-867, 1987.

71. Neymark, L.A., Holm-Denoma, C.S. and Moscati, R.J.: In situ LA-ICPMS U–Pb dating of cassiterite without a known-age matrix-matched reference material: Examples from worldwide tin deposits spanning the Proterozoic to the Tertiary. *Chemical Geology*, *483*, 410-425, 2018.
72. Nicholson, S.L., Pike, A.W., Hosfield, R., Roberts, N.M.W., Sahy, D., Woodhead, J., Cheng, H., Edwards, R.L., Affolter, S., Leuenberger, M. and Burns, S.J., 2020. Pluvial periods in Southern Arabia over the last 1.1 million-years. *Quaternary Science Reviews*, *229*, DOI:10.1016/j.quascirev.2019.106112.
73. Nuriel, P., Craddock, J., Kylander-Clark, A.R., Uysal, T., Karabacak, V., Dirik, R.K., Hacker, B.R. and Weinberger, R.: Reactivation history of the North Anatolian fault zone based on calcite age-strain analyses. Geology, 47, 465-469, 2019.
74. Nuriel, P., Weinberger, R., Kylander-Clark, A.R.C., Hacker, B.R. and Craddock, J.P.: The onset of the Dead Sea transform based on calcite age-strain analyses. Geology, 45, 587-590, 2017.
75. Osmond, J.K. and Cowart, J.B.: Ground water, in: Uranium-series Disequilibrium: Applications to Earth, Marine, and Environmental Sciences, Second Edition, edited by: Ivanovich, M. and Harmon, R.S., Clarendon Press, Oxford, UK, 290-330.
76. Osmond, J.K. and Cowart, J.B.: The theory and uses of natural uranium isotopic variations in hydrology. *Atomic Energy Review*, *14*, 621-679, 1976.
77. Osmond, J.K. and Cowart, J.B.: U-series nuclides as tracers in groundwater hydrology, in: *Environmental tracers in subsurface hydrology, edited by* Cook P.G., and Herczeg A.L., Springer, Boston, MA, USA, 145-173, 2000.
78. Osmond, J.K., Rydell, H.S. and Kaufman, M.I.: Uranium disequilibrium in groundwater: an isotope dilution approach in hydrologic investigations. *Science*, *162*, 997-999, 1968.
79. Palin, R.M., Searle, M.P., Waters, D.J., Parrish, R.R., Roberts, N.M.W., Horstwood, M.S.A., Yeh, M.W., Chung, S.L. and Anh, T.T.: A geochronological and petrological study of anatectic paragneiss and associated granite dykes from the Day Nui C on Voi metamorphic core complex, North Vietnam: constraints on the timing of metamorphism within the Red River shear zone. *Journal of Metamorphic Geology*, *31*, 359-387, 2013.
80. Pagel, M., Bonifacie, M., Schneider, D.A., Gautheron, C., Brigaud, B., Calmels, D., Cros, A., Saint-Bezar, B., Landrein, P., Sutcliffe, C. and Davis, D.: Improving paleohydrological and diagenetic reconstructions in calcite veins and breccia of a

sedimentary basin by combining Δ47 temperature, $\delta^{18}O_{water}$ and U-Pb age. Chemical Geology, 481, 1-17, 2018.

81. Paquette, J. and Reeder, R.J.: Relationship between surface structure, growth mechanism, and trace element incorporation in calcite. *Geochimica et Cosmochimica Acta*, *59*, 735-749, 1995.
82. Parrish, R.R., Parrish, C.M. and Lasalle, S.: Vein calcite dating reveals Pyrenean orogen as cause of Paleogene deformation in southern England. Journal of the Geological Society, 175, 425-442, 2018.
83. Paton, C., Hellstrom, J., Paul, B., Woodhead, J. and Hergt, J.: Iolite: Freeware for the visualisation and processing of mass spectrometric data. *Journal of Analytical Atomic Spectrometry*, *26*, 2508-2518, 2011.
84. Paton, C., Woodhead, J.D., Hellstrom, J.C., Hergt, J.M., Greig, A. and Maas, R.: Improved laser ablation U-Pb zircon geochronology through robust downhole fractionation correction. *Geochemistry, Geophysics, Geosystems*, *11*, Q0AA06, DOI:10.1029/2009GC002618, 2010.
85. Perrette, Y., Delannoy, J.J., Desmet, M., Lignier, V. and Destombes, J.L.: Speleothem organic matter content imaging. The use of a Fluorescence Index to characterise the maximum emission wavelength. *Chemical Geology*, *214*, 193-208, 2005.
86. Petrus, J.A., Chew, D.M., Leybourne, M.I. and Kamber, B.S.: A new approach to laser-ablation inductively-coupled-plasma mass-spectrometry (LA-ICP-MS) using the flexible map interrogation tool 'Monocle'. *Chemical Geology*, *463*, 76-93, 2017.
87. Pevear, D.R., Vrolijk, P.J., Longstaffe, F.J., Hendry, J., Carey, P., Parnell, J., Ruffell, A. and Worden, R.: Timing of Moab fault displacement and fluid movement integrated with burial history using radiogenic and stable isotopes. *Geofluids II*, *97*, 42-45, 1997.
88. Pickering, R., Kramers, J.D., Partridge, T., Kodolanyi, J. and Pettke, T.: U–Pb dating of calcite–aragonite layers in speleothems from hominin sites in South Africa by MC-ICP-MS. *Quaternary Geochronology*, *5*, 544-558, 2010.
89. Porcelli, D. and Swarzenski, P.W.: The behavior of U-and Th-series nuclides in groundwater. *Reviews in Mineralogy and Geochemistry*, *52*, 317-361, 2003.
90. Quade, J., Rasbury, E.T., Huntington, K.W., Hudson, A.M., Vonhof, H., Anchukaitis, K., Betancourt, J., Latorre, C. and Pepper, M.: Isotopic characterization of late

Neogene travertine deposits at Barrancas Blancas in the eastern Atacama Desert, Chile. *Chemical Geology*, *466*, 41-56, 2017.

91. Rasbury, E.T. and Cole, J.M.: Directly dating geologic events: U-Pb dating of carbonates. *Reviews of Geophysics*, *47*, 2009.
92. Rasbury, E.T., Hanson, G.N., Meyers, W.J. and Saller, A.H.: Dating of the time of sedimentation using U-Pb ages for paleosol calcite. *Geochimica et Cosmochimica Acta*, *61*, 1525-1529, 1997.
93. Ray, J.S., Veizer, J. and Davis, W.J.: C, O, Sr and Pb isotope systematics of carbonate sequences of the Vindhyan Supergroup, India: age, diagenesis, correlations and implications for global events. *Precambrian Research*, *121*, 103-140, 2003.
94. Reeder, R.J.: Interaction of divalent cobalt, zinc, cadmium, and barium with the calcite surface during layer growth. *Geochimica et Cosmochimica Acta*, *60*, 1543-1552, 1996.
95. Reeder, R.J., Nugent, M., Lamble, G.M., Tait, C.D. and Morris, D.E.: Uranyl incorporation into calcite and aragonite: XAFS and luminescence studies. *Environmental Science & Technology*, *34*, 638-644, 2000.
96. Reeder, R.J., Nugent, M., Tait, C.D., Morris, D.E., Heald, S.M., Beck, K.M., Hess, W.P. and Lanzirotti, A.: Coprecipitation of uranium (VI) with calcite: XAFS, micro-XAS, and luminescence characterization. *Geochimica et Cosmochimica Acta*, *65*, 3491-3503, 2001.
97. Regis, D., Warren, C.J., Mottram, C.M. and Roberts, N.M.W.: Using monazite and zircon petrochronology to constrain the P–T–t evolution of the middle crust in the Bhutan Himalaya. *Journal of Metamorphic Geology*, *34*, 617-639, 2016.
98. Richards, D.A., Bottrell, S.H., Cliff, R.A., Ströhle, K. and Rowe, P.J.: U-Pb dating of a speleothem of Quaternary age. *Geochimica et Cosmochimica Acta*, *62*, 3683-3688, 1998.
99. Richter, D.K., Götte, T., Götze, J. and Neuser, R.D.: Progress in application of cathodoluminescence (CL) in sedimentary petrology. *Mineralogy and Petrology*, *79*, 127-166, 2003.
100. Ring, U. and Gerdes, A.: Kinematics of the Alpenrhein-Bodensee graben system in the Central Alps: Oligocene/Miocene transtension due to formation of the Western Alps arc. Tectonics, 35, 1367-1391, 2016.

101. Roberts, N.M.W., Rasbury, E.T., Parrish, R.R., Smith, C.J., Horstwood, M.S.A. and Condon, D.J.: A calcite reference material for LA-ICP-MS U-Pb geochronology. Geochemistry, Geophysics, Geosystems, 18, 2807-2814, 2017.
102. Roberts, N.M.W. and Walker, R.J.: U-Pb geochronology of calcite-mineralized faults: Absolute timing of rift-related fault events on the northeast Atlantic margin. Geology, 44, 531-534, 2016.
103. Robertson, K., Gauvin, R. and Finch, J.: Application of charge contrast imaging in mineral characterization. *Minerals Engineering*, *18*, 343-352, 2005.
104. Romer, R.L. and Wright, J.E., 1993. Lead mobilization during tectonic reactivation of the western Baltic Shield. *Geochimica et Cosmochimica Acta*, *57*, 2555-2570.
105. Russell, J., Chadwick, B., Rao, B.K. and Vasudev, V.N.: Whole-rock PbPb isotopic ages of Late Archaean limestones, Karnataka, India. *Precambrian Research*, *78*, 261-272, 1996.
106. Sarangi, S., Gopalan, K. and Kumar, S.: Pb–Pb age of earliest megascopic, eukaryotic alga bearing Rohtas Formation, Vindhyan Supergroup, India: implications for Precambrian atmospheric oxygen evolution. *Precambrian Research*, *132*, 107-121, 2004.
107. Savard, M.M., Veizer, J. and Hinton, R.: Cathodoluminescene at low Fe and Mn concentrations; a SIMS study of zones in natural calcites. *Journal of Sedimentary Research*, *65*, 208-213, 1995.
108. Scardia, G., Parenti, F., Miggins, D.P., Gerdes, A., Araujo, A.G. and Neves, W.A.: Chronologic constraints on hominin dispersal outside Africa since 2.48 Ma from the Zarqa Valley, Jordan. *Quaternary Science Reviews*, *219*, 1-19, 2019.
109. Shopov, Y.Y., Ford, D.C. and Schwarcz, H.P.: Luminescent microbanding in speleothems: high-resolution chronology and paleoclimate. *Geology*, *22*, 407-410, 1994.
110. Smeraglia, L., Aldega, L., Billi, A., Carminati, E., Di Fiore, F., Gerdes, A., Albert, R., Rossetti, F. and Vignaroli, G.: Development of an intra-wedge tectonic mélange by out-of-sequence thrusting, buttressing, and intraformational rheological contrast, Mt. Massico ridge, Apennines, Italy. Tectonics, 38, 1223-1249, 2019.
111. Smith, P.E. and Farquhar, R.M.: Direct dating of Phanerozoic sediments by the 238U–206Pb method. *Nature*, *341*, 518, 1989.

112. Smith, P.E., Farquhar, R.M. and Hancock, R.G.: Direct radiometric age determination of carbonate diagenesis using U-Pb in secondary calcite. *Earth and Planetary science letters*, *105*, 474-491, 1991.
113. Solum, J.G., van der Pluijm, B.A. and Peacor, D.R.: Neocrystallization, fabrics and age of clay minerals from an exposure of the Moab Fault, Utah. *Journal of Structural Geology*, *27*, 1563-1576, 2005.
114. Stacey, J.T. and Kramers, J.: Approximation of terrestrial lead isotope evolution by a two-stage model. *Earth and planetary science letters*, *26*, 207-221, 1975.
115. Stübner, K., Grujic, D., Parrish, R.R., Roberts, N.M., Kronz, A., Wooden, J. and Ahmad, T.: Monazite geochronology unravels the timing of crustal thickening in NW Himalaya. *Lithos*, *210*, 111-128, 2014.
116. Sturchio, N.C., Antonio, M.R., Soderholm, L., Sutton, S.R. and Brannon, J.C.: Tetravalent uranium in calcite. *Science*, *281*, 971-973, 1998.
117. Suksi, J., Rasilainen, K. and Pitkänen, P.: Variations in 234U/238U activity ratios in groundwater—A key to flow system characterisation?. *Physics and Chemistry of the Earth, Parts A/B/C*, *31*, 556-571, 2006.
118. Sumner, D.Y. and Bowring, S.A.: U-Pb geochronologic constraints on deposition of the Campbellrand Subgroup, Transvaal Supergroup, South Africa. *Precambrian Research*, *79*, 25-35, 1996.
119. Taylor, P.N. and Kalsbeek, F.: Dating the metamorphism of Precambrian marbles: Examples from Proterozoic mobile belts in Greenland. *Chemical Geology: Isotope Geoscience Section*, *86*, 21-28, 1990.
120. Trudgill, B.D.: Evolution of salt structures in the northern Paradox Basin: Controls on evaporite deposition, salt wall growth and supra-salt stratigraphic architecture. *Basin Research*, *23*, 208-238, 2011.
121. Tullborg, E.L., Drake, H. and Sandström, B.: Palaeohydrogeology: a methodology based on fracture mineral studies. *Applied Geochemistry*, *23*, 1881-1897, 2008.
122. Ukar, E. and Laubach, S.E.: Syn-and postkinematic cement textures in fractured carbonate rocks: Insights from advanced cathodoluminescence imaging. *Tectonophysics*, *690*, 190-205, 2016.
123. Uysal, I.T., Feng, Y.X., Zhao, J.X., Bolhar, R., Işik, V., Baublys, K.A., Yago, A. and Golding, S.D.: Seismic cycles recorded in late Quaternary calcite veins: geochronological, geochemical and microstructural evidence. *Earth and Planetary Science Letters*, *303*, 84-96, 2011.

124. Walter, B.F., Gerdes, A., Kleinhanns, I.C., Dunkl, I., von Eynatten, H., Kreissl, S. and Markl, G.: The connection between hydrothermal fluids, mineralization, tectonics and magmatism in a continental rift setting: Fluorite Sm-Nd and hematite and carbonates U-Pb geochronology from the Rhinegraben in SW Germany. Geochimica et Cosmochimica Acta, 240, 11-42, 2018.
125. Warren, C.J., Singh, A.K., Roberts, N.M.W., Regis, D., Halton, A.M. and Singh, R.B.: Timing and conditions of peak metamorphism and cooling across the Zimithang Thrust, Arunachal Pradesh, India. *Lithos*, *200*, 94-110, 2014.
126. Watt, G.R., Griffin, B.J. and Kinny, P.D.: Charge contrast imaging of geological materials in the environmental scanning electron microscope. *American Mineralogist*, *85*, 1784-1794, 2000.
127. Weremeichik, J.M., Gabitov, R.I., Thien, B.M. and Sadekov, A.: The effect of growth rate on uranium partitioning between individual calcite crystals and fluid. *Chemical Geology*, *450*, 145-153, 2017.
128. Wendt, I. and Carl, C.: The statistical distribution of the mean squared weighted deviation. *Chemical Geology: Isotope Geoscience Section*, *86*, 275-285, 1991.
129. Whitehouse, M.J. and Russell, J.: Isotope systematics of Precambrian marbles from the Lewisian complex of northwest Scotland: implications for Pb□ Pb dating of metamorphosed carbonates. *Chemical Geology*, *136*, 295-307, 1997.
130. Williams, R.T., Goodwin, L.B., Sharp, W.D. and Mozley, P.S.: Reading a 400,000-year record of earthquake frequency for an intraplate fault. *Proceedings of the National Academy of Sciences*, *114*, 4893-4898, 2017.
131. Woodhead, J., Hellstrom, J., Maas, R., Drysdale, R., Zanchetta, G., Devine, P. and Taylor, E.: U–Pb geochronology of speleothems by MC-ICPMS. *Quaternary Geo*chronology, 1, 208-221, 2006.
132. Woodhead, J., Hellstrom, J., Pickering, R., Drysdale, R., Paul, B. and Bajo, P.: U and Pb variability in older speleothems and strategies for their chronology. *Quaternary Geochronology*, *14*, 105-113, 2012.
133. Woodhead, J. and Petrus, J., 2019. Exploring the advantages and limitations of in situ U–Pb carbonate geochronology using speleothems. *Geochronology*, *1*, 69-84.
134. Woodhead, J.D., Sniderman, J.K., Hellstrom, J., Drysdale, R.N., Maas, R., White, N., White, S. and Devine, P.: The antiquity of Nullarbor speleothems and implications for karst palaeoclimate archives. *Scientific reports*, *9*, 603, 2019.

135. Yokoyama, T., Kimura, J.I., Mitsuguchi, T., Danhara, T., Hirata, T., Sakata, S., Iwano, H., Maruyama, S., Chang, Q., Miyazaki, T. and Murakami, H.: U-Pb dating of calcite using LA-ICP-MS: Instrumental setup for non-matrix-matched age dating and determination of analytical areas using elemental imaging. Geochemical Journal, 52, 531-540, 2018.